# ELASTO-PLASTIC IMPACT OF A CANTILEVER BEAM USING NON-LINEAR FINITE ELEMENTS AND EVENT SIMULATION

by

Todd C. Werner

Submitted in Partial Fulfillment of the Requirements

for the Degree of

Master of Science in Engineering

in the

Mechanical Engineering Program

YOUNGSTOWN STATE UNIVERSITY

August 1998

# ELASTO-PLASTIC IMPACT OF A CANTILEVER BEAM USING NON-LINEAR FINITE ELEMENTS AND EVENT SIMULATION

Todd C. Werner

I hereby release this thesis to the public. I understand this thesis will be housed at the Circulation Desk of the University library and will be available for public access. I also authorize the University or other individuals to makes copies of this thesis as needed for scholarly research.

Signature:

Todd C. Werner 8/14/98

Student Date

Approvals:

Daniel H. Suchow 8/14/98

Thesis Advisor Date

Robert A. McCoy 8-14-98

Committee Member Date

Edgar W. Kiser 8-14-98

Committee Member Date

Peter J. Rasvinski 8/17/98

Dean of Graduate Studies Date

# Abstract

The objective of this study was to use a personal computer based nonlinear finite element analysis / event simulation software package by Algor, Inc. to simulate and analyze the transverse elasto-plastic impact of a cantilever beam due to a free falling object striking the free end of the beam. The results of the computer analysis were compared to results of actual laboratory impact tests. Based upon these comparisons, the accuracy / validity of the economical PC based software was evaluated. There are approximation methods and closed form solutions to impact problems within the elastic limit, however, these methods are only applicable for simple geometries. Currently, no closed form mathematical solutions to post yield impact problems. The PC based software, due to its affordability, can provide a solution method for such problems to the general engineering population.

## Acknowledgments

I would like to take this opportunity to show my appreciation and give my sincerest thanks to the follow people for all that they have provided.

First and foremost my wife and best friend, Amy S. Werner, whose emotional and financial support along with her love and belief in me made this a reality.

My daughter, Samantha A. Werner, who is the new center of my universe. Her bright smiling face makes me realize what is truly important in life.

My parents, Charles H. and Linda B. Werner, who have always encouraged me to pursue my hopes and dreams and to never lose faith.

My siblings, Ryan K. and Whitney L. Werner, whose words of encouragement and support mean more to me than they realize.

My in-laws, Donald C., Mary I., Daniel G., and Andrea L. Musser, who made me a part of their family years ago.

Dr. Daniel H. Suchora - Thesis Advisor, who provided a great deal of assistance, persistence, and advice.

Dr. Shawn (H. Y.) Kim - Department Chairman, Graduate Committee

Dr. Robert A. M$^{c}$Coy - Graduate Committee

Mr. Anirban Mukherjee - Graduate Student

Mr. Bill Challis and Mr. Joe Argyros - Satec Systems, Inc., Grove City, PA

# Table of Contents

**Chapter 1: Introduction** . . . . . 1

**Chapter 2: Theoretical Analysis and Literary Review** . . . . . 4
- 2.1: Introduction . . . . . 4
- 2.2: Definition of Impact . . . . . 5
- 2.3: Types of Impact . . . . . 6
- 2.4: Energy Approximation Method - The Static Equivalent Load . . . . . 6
- 2.5: Longitudinal Waves in Elastic Media . . . . . 10
- 2.6: Theoretical Basis of Event Simulation . . . . . 15

**Chapter 3: Experimental Material Testing** . . . . . 21

**Chapter 4: Finite Element Analysis / Event Simulation** . . . . . 27

**Chapter 5: Experimental Verification** . . . . . 36

**Chapter 6: Results and Conclusions** . . . . . 45
- 6.1: Results . . . . . 45
- 6.2: Conclusions . . . . . 50

**References** . . . . . 51

**Appendix A: Satec EMF 33 Tensile Tester Verification Sheets** . . . 53

**Appendix B: Algor Decoder Settings** . . . . . 56

**Appendix C: Laboratory Equipment Utilized** . . . . . 60

# List of Figures

**Figure 1.1** - Computer simulation of an offset frontal crash test of a BMW. . . . . 2

**Figure 1.2** - Frontal crash simulation of a BMW at maximum deflection. . . . . 2

**Figure 1.3** - System used in experimental and computational methods discussed. Cantilever beam shown with electrical resistance strain gage and free falling impacting mass. . . . . 3

**Figure 2.5.1** - Forces and displacements on an element of an elastic bar. . . . . 11

**Figure 2.5.2** - Travel of $\Delta x$ of the value function $f$ in time increment $\Delta t$. . . . . 12

**Figure 2.5.3** - Strains and corresponding stresses in
(a) a positive wave - propagating to the right;
(b) a negative wave - propagating to the left. . . . . 13

**Figure 2.6.1** - Typical cantilever beam with a load F on the free end. . . . . 16

**Figure 2.6.2** - Diagram representing a typical spring-mass-damper system. . . . . 20

**Figure 3.1** - Drawing of tensile specimen for sheet material as specified by 1980 Annual Book of ASTM Standards Part 10: Metals - Physical, Mechanical, Corrosion Testing. . . . . 22

**Figure 3.2** - Sample 1. Stress vs. strain curve output from SATEC Systems, Inc. tensile test machine and software interface. . . . . 23

**Figure 3.3** - Sample 2. Stress vs. strain curve output from SATEC Systems, Inc. tensile test machine and software interface. . . . . 24

**Figure 3.4** - Sample 3. Stress vs. strain curve output from SATEC Systems, Inc. tensile test machine and software interface. . . . . 25

**Figure 4.1** - The FEA model used to simulate the impact of a free falling mass. The aluminum beam is shown in green, the full constraint boundary conditions are in red, and the impacting mass is shown in gold. . . . . 27

**Figure 4.2** - The basic formulation of a 3-D element. Note the node numbering and the local coordinate systems. The 20 node brick is formed by extruding this figure into its third dimension. . . . . 29

**Figure 4.3** - The basic formulation of a 20 node brick 29

**Figure 4.4** - The initial impact at time t = 0. - No damping. . . . . 31

**Figure 4.5** - Just after impact at time t = 0.0125 sec. - No damping. . . . . 32

**Figure 4.6** - The displacement due to impact at time t = 0.025. - No damping. . . . 32

**Figure 4.7** - The displacement due to impact at time t = 0.0375 sec. - No damping 33

**Figure 4.8** - The point of maximum deflection. Time t = 0.0565 sec. No damping. . . . . 33

**Figure 4.9** - Isometric view of the flexural stress distribution over the top surface. No damping. . . . . 34

**Figure 4.10** - Isometric view of the longitudinal strain distribution over the top surface. No damping. . . . . 34

**Figure 5.1** - The experimental system set up. . . . . 36

**Figure 5.2** - Personal computer and SDA 2000 data acquisition unit. . . . . 37

**Figure 5.3** - Strain indicators attached to test beam strain gages. . . . . 37

**Figure 5.4** - The weight aligned with the end of the cantilever beam. . . . . 38

**Figure 5.5** - Typical CEA series gage showing the backing, copper tabs, encapsulation, and grid. . . . . 38

**Figure 5.6** - Nomenclature for a typical CEA series gage. . . . . 39

**Figure 5.7** - Diagram of a three wire circuit for a single active gage Wheatstone quarter bridge. . . . . 39

**Figure 5.8** - Graphical output of strain gage calibration using a static load. . . . . 41

**Figure 5.9** - Graphical output of strain gage calibration using strain indicator internal shunt. . . . . 42

**Figure 5.10** - Trial #2 captured data. . . . . 43

**Figure 5.11** - Trial #2 captured data - initial impact enlarged. . . . . 43

**Figure 6.1.1** - Stress vs. strain curve showing what FEA stress should be predicted based on the strain values FEA models predicted. . . . . 46

**Figure 6.1.2** - Graph of strain vs. time for the FEA models and experimental data. 49

# List of Tables

**Table 3.1** - Physical dimensions of the test specimens. . . . . 22

**Table 3.2** - Results of tensile tests. . . . . 26

**Table 4.1** - Maximum strain results at gage locations in FEA models. . . . . 35

**Table 4.2** - Maximum flexural stress results at gage locations in FEA models. . . . . 35

**Table 5.1** - Maximum dynamic strain results at gage locations in the experimental trials. . . . . 44

**Table 6.1.1** - Maximum strain results at gage locations in FEA models. . . . . 45

**Table 6.1.2** - Maximum dynamic strain results at gage locations in the experimental trials. . . . . 45

**Table 6.1.3** - Maximum flexural stress results at gage locations in FEA models. . . . . 46

**Table 6.1.4** - Comparison of undamped FEA stress to values from $\sigma$ vs. $\varepsilon$ curve for the FEA predicted strain values. . . . . 47

**Table 6.1.5** - Comparison of damped FEA stress to values from $\sigma$ vs. $\varepsilon$ curve for the FEA predicted strain values. . . . . 47

**Table 6.1.6** - Comparison of FEA with no damping to the average experimental results. . . . . 47

**Table 6.1.7** - Comparison of FEA with damping to the average experimental results. 47

# Chapter 1: Introduction

Since man began to study the fundamental mechanics of the world we live in, accurate closed form mathematical solutions to simple impact problems have been extremely difficult to develop. As the impact scenario becomes more complex, the possibility of a closed form mathematical solution becomes even more remote. If plastic deformation occurs or a nonlinear elastic material is used an accurate closed form solution is nearly impossible.

Approximate methods have been developed to help engineers obtain information about impact problems. Typically these methods utilize energy balances to find static equivalent loads for the impact event. These methods ignore the stress waves that propagate within a member in a typical impact situation and in some instances are grossly in error. These work relatively well within the elastic region of an isotropic material, but were essentially useless in the plastic region or for a non-isotropic materials. These estimated results along with a generous design factor would often lead to a functional yet perhaps overdesigned component.

Numerical solutions to the actual governing equations of an impact event have been developed, however, these require powerful computer resources to solve even simple problems. These numerical methods have allowed solutions to be obtained on large scale computers. Engineers in the automotive world which have powerful computer systems have the capability to accurately solve many difficult problems including elasto-plastic impact situations. The ability to simulate a crash (impact) test on a computer greatly reduces costs by eliminating the need for full scale prototypes and allowing

changes to be made before a unit is ever put into production. Similarly, savings are realized by reducing concept to production time and consumer safety is increased by structural refinements that can be made due to simulated crashes. According to Ford Motor Co., the ability to predict this type of impact behavior represents a "most fundamental change of the engineering."

> 09/05/96 - New Ford Computers Allow $10 Crash Simulations
>
> Dearborn, Michigan - Ford Motor Co. has launched a new computer-aided design (CAD) project that could enable the automaker to conduct simulated vehicle frontal crash tests for only about $10, reports Reuters. In past years, automakers had to physically crash large numbers of vehicles to ensure safety - but now computers can analyze crashes while still in the design stage, when changes can be made more economically. Ford says the new program represents the most fundamental change of the engineering computer infrastructure in Ford's history. With the new system, Ford also plans to eliminate 90 percent of its physical prototypes by the year 2000 in favor of the electronic versions. The C3P project is expected to cut prototype costs up to 50 percent and eliminate half the costly changes that occur late in the development process.[1]

Figures 1.1 and 1.2 show examples of how this technology is being applied in the automotive industry.

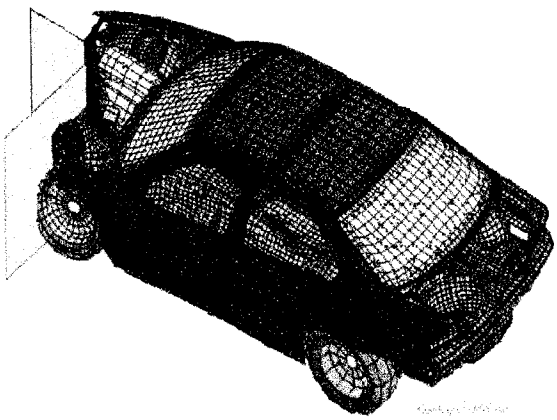

**Figure 1.1** - Computer simulation of an offset frontal crash test of a BMW.[2]

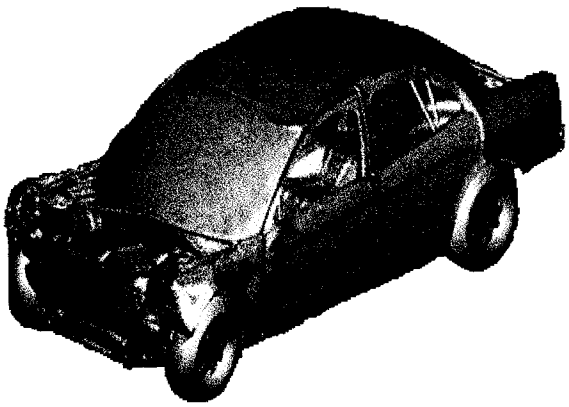

**Figure 1.2** - Frontal crash simulation of a BMW at maximum deflection.[3]

---

[1] A Ford Motor Co. press release from September 5, 1996

[2] This picture was obtained from a publicly accessible internet site and it is assumed to be in the public domain for public use. http://www.esi.fr/

[3] Automotive Engineering International, May 1998. Pg. 36

The focus of this work is a free falling mass impacting on the free end of a cantilevered beam (Figure 1.3). The problem is solved in two ways. First, a non-linear computer simulation of the impact event is performed on an affordable personal computer using the economical software package, Algor. Then actual experimental data is collected from the impact of test beams mounted with electrical resistance strain gages dynamically recording impact strains. Finally, the results of the computer simulations are compared to the actual dynamic strains recorded in the laboratory tests to verify the validity and accuracy of the computer model.

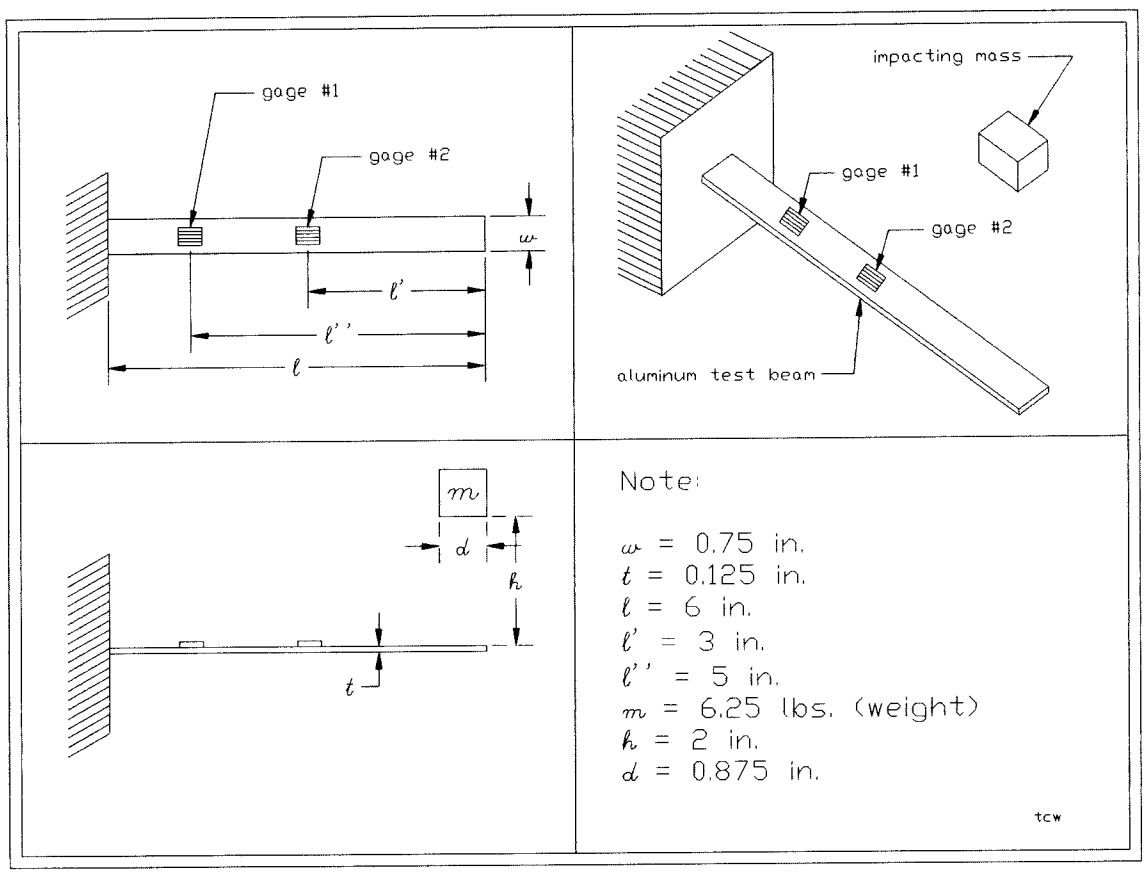


**Figure 1.3** - System used in experimental and computational methods discussed. Cantilever beam shown with electrical resistance strain gage and free falling impacting mass.

# Chapter 2: Theoretical Analysis and Literary Review

## 2.1 Introduction

In this chapter impact is defined and several types of impact problems are discussed. Two primary solution approximation methods, simplified equivalent static loading and stress wave propagation, are presented as results of past work on impact problems. The static equivalent loading method is somewhat easy to apply to a wide range of problems, but at times accuracy is poor. The stress wave propagation technique is highly accurate, but can be extremely mathematically complex for even the simplest of problems and impossible for more complex situations. These approximation techniques are typically accurate only for small deflections within the elastic range of a homogenous isotropic material. Once the material has reach its yield point or if the material is of a nonlinear elastic nature, the validity of these solution methods no longer applies. These types of situations will now simply be referred to as nonlinear.

Until recently if a nonlinear impact situation was being investigated, the engineer involved had few options of recourse. The solutions mentioned above may be employed with a design factor based on previous experience. Time consuming and costly laboratory prototyping could be used or complex plasticity theory may be used by an engineer specializing in this area.

Today, nonlinear finite element analysis and event simulation solutions as well as virtual engineering and prototyping are becoming available to the majority of the engineering population. The solution method behind Algor Inc.'s nonlinear event simulation software Accupak/VE module will also be

discussed in this chapter and later used to predict the results of experimental laboratory impact tests performed on the cantilever beams.

## 2.2 Definition of Impact

Typically, impact is defined as two or more bodies colliding with each other during a very short time interval, causing large impulsive forces to be exerted between the bodies. The force application time interval mentioned is more clearly defined as a "duration of load application less than one-half the fundamental natural period of vibration of the member upon which the force acts." [1] However, if the time of loading exceeds three times the fundamental natural period of vibration, dynamic effects are considered negligible and static loading may be assumed. A "gray area" exists between one-half and three times the fundamental natural period of vibration in which a quasi-static or quasi-dynamic approach may be used.[2]

Under elastic impact two factors must be considered. First, energy is not conserved, however this assumption is often used to simplify the mathematics involved in a solution. Secondly, momentum is conserved. This fact can be applied to the system before and after impact to determine a ratio of the relative velocities before and after the collision known as the coefficient of restitution, $e$. The coefficient of restitution between two known materials can be used when using static equivalent loading to adjust for the system energy not being conserved. The value of the coefficient of restitution varies from $0 < e < 1$, with 0 being a perfectly plastic collision (no rebound and parts stick and travel together), and 1 being a perfectly elastic collision

---

[1] Mark's Standard Handbook for Mechanical Engineers - 10th Edition. Pg. 5-43
[2] Fundamentals of Machine Component Design - 2nd Edition. Pg. 236

(complete rebound). Most physical situations occur between these two extremes.

## 2.3 Types of Impact

Three main types of impact exist; (1) axial (2) torsional (3) transverse. These can cause uniform tension or compression stresses, shearing stresses, or bending stresses. *Axial (longitudinal) impact* occurs in mechanisms such as hoisting ropes and cables, coupling-connected railroad cars, and helical springs. *Torsional impact* occurs in items like rotating shafts, geared drives, clutches and brakes, and drills. *Transverse (bending) impact* occurs in shafts and structural members such as beams and plates.

These three types can be further classified as *striking impact* or *force impact*. Striking impact involves bodies striking or colliding with each other. Force impact occurs when a force or torque is rapidly applied like the friction in a clutch or in the sudden support of the weight of a body. These types of impact can occur in combination. The free falling mass impacting the cantilevered beam in this study is a combination of striking (due to the collision) and force (due to the addition of the mass to the end of the beam for a short time) impact. The impact in this study could then be described as striking/force transverse impact on the free end of a cantilever beam.

## 2.4 The Energy Approximation Method - The Static Equivalent Load

The most basic technique for impact analysis is the static equivalent load approximation. This method employs the use of an energy balance to determine a static load that would produce the same maximum deflection as the lesser force in the impact case. There are several assumptions built into

the static equivalent load approximation to make it solvable. They are (1) energy is conserved and is completely transferred between bodies, (2) mass of the structure is negligible, (3) deflections within the mass itself are negligible, (4) damping within the system is negligible, (5) vibrational stress waves are ignored, (6) all deflections remain in the elastic region. These assumption have important implications when being applied.

1. The second assumption implies that the dynamic deflection curve is the same as the static deflection curve, multiplied by an impact load factor. Actually the dynamic deflection curve will inevitability involve points of higher local strain due to the rapid rate of load application.

2. *Some* deflection will always occur within the mass itself, and in doing so, a portion of the energy of the system will be absorbed. Therefore, in reality, assumptions (1) and (3) will always be violated, causing the strains in the structure to be *slightly lower* than calculated.

3. Any physical case will involve *some* damping in the form of friction, windage, internal damping due to structural deflection, etc. Depending on the degree that these are present, the actual strains may be *significantly lower* than the calculated values. Assumption (4) will always be violated.

4. Under impact, vibrational waves are generated. This is what causes "ringing" in bells and other similar items when they are struck. The degree to which these waves exist is dependent upon the amount of damping present. More damping allows less vibration and vice versa. These waves can cause a magnification effect, thereby causing the actual stress values to be *significantly greater* than calculated values.

5. Assumption (6) states that this method is developed on the basis that the material(s) involved is linearly elastic. If during impact, the yield point is exceeded or the material(s) are of a nonlinear / non-isotropic nature, then this method will be in error.

Keeping the above statements in mind, the static equivalent load approximation is developed as follows.

First, apply Hooke's law:

$$F_{st} = k\delta \qquad \text{Eq. (2.4.1)}$$

where:

$F_{st}$ is the static equivalent load to cause the same deflection as impact

$k$ is Hooke's elastic spring constant of the structure

$\delta$ is the deflection caused by impact.

Now,

$$\delta_{st} = \frac{W}{k} \qquad \text{Eq. (2.4.2)}$$

where:

$\delta_{st}$ is the static deflection that would be caused by W with no impact

W is the weight of the impacting mass

$k$ is Hooke's elastic spring constant of the structure.

Now equating the potential energy lost by the mass falling from a height $h$ to the energy absorbed by the structure gives:

(Energy lost by the mass) = (Work done on the structure)

$$W(h+\delta) = \int_{\delta} F_{st}\, d\delta \qquad \text{Eq. (2.4.3)}$$

Since the Force vs. Deflection is assumed to be linear in this case, equation (2.4.3) can be integrated to give

$$W(h+\delta) = \tfrac{1}{2} F_{st}\delta \qquad \text{Eq. (2.4.3a)}$$

Solving for $k$ simultaneously in equations (2.4.1) and (2.4.2) above yields:

$$F_{st} = \left(\frac{\delta}{\delta_{st}}\right)W \text{ or } \left(\frac{\delta}{\delta_{st}}\right) = \frac{F_{st}}{W} \qquad \text{Eq. (2.4.4a \& b)}$$

Substituting Eq. (2.4.4a) into Eq. (2.4.3) gives:

$$W(h+\delta) = \frac{1}{2}\frac{\delta^2}{\delta_{st}}W \qquad \text{Eq. (2.4.5)}$$

Equation (2.4.5) is a quadratic in terms of δ, which is solved as:

$$\delta = \delta_{st}\left(1+\sqrt{1+\frac{2h}{\delta_{st}}}\right) \qquad \text{Eq. (2.4.6)}$$

Likewise, substituting Eq. (2.4.4b) into Eq. (2.4.3) gives:

$$F_{st} = W\left(1+\sqrt{1+\frac{2h}{\delta_{st}}}\right) \qquad \text{Eq. (2.4.7)}$$

The value in the parenthesis of equations (2.4.6) and (2.4.7) is often referred to as the *impact factor*. This is the amount that the weight of the mass or the deflection it would give statically is multiplied by to obtain the static equivalent impact force or impact deflection.

The above development could also be done in terms of velocity due to free fall by substituting: $v^2 = 2gh$ or $h = \frac{v^2}{2g}$ where $g$ is acceleration of gravity.

$$\delta = \delta_{st}\left(1+\sqrt{1+\frac{v^2}{g\delta_{st}}}\right) \qquad \text{Eq. (2.4.6a)}$$

$$F_{st} = W\left(1 + \sqrt{1 + \frac{v^2}{g\delta_{st}}}\right) \qquad \text{Eq. (2.4.7a)}$$

Two items should be noted from the above equations. First, if the free fall height *h* is reduced to zero, the impact factor becomes 2, which is the accepted multiplication factor for a *suddenly applied* load. Secondly, the relationship of the structure to $\delta_{st}$ must be known. For basic beams these can be found in stress analysis texts or other references like Roark's Formulas for Stress and Strain.

Energy loss factors, K, may also be used to account for the system's energy not being conserved. Typically these values are empirically determined for various structures and may be applied cautiously to similar situations. For a cantilever beam transversely impacted by a falling mass on its free end, Roark's Formulas for Stress and Strain[3] lists a factor of K of

$$K = \frac{1 + \frac{33}{140}\frac{M_1}{M}}{\left(1 + \frac{3}{8}\frac{M_1}{M}\right)^2} \qquad \text{where:}$$

$M_1$ is the mass of the cantilever beam, and

M is the impacting mass.

## 2.5 Longitudinal Waves in Elastic Media

As mentioned in the previous section, under impact, vibrational waves are generated. This is what causes "ringing" in bells and other similar items when they are struck.

During wave propagation in a long bar, it is assumed that particles in

[3] Roark's Formulas for Stress and Strain - 6th Edition. Pg. 719.

any normal section move along together through parallel planes. Their displacement $u$ is then a function of position $x$ and time $t$, $u = f(x,t)$. The change in length of the element is simply $\left(\frac{\partial u}{\partial x}\right)dx$, then the unit strain is $\left(\frac{\partial u}{\partial x}\right)$. The stress by Hooke's law becomes $\sigma = E\left(\frac{\partial u}{\partial x}\right)$ and the corresponding force in that section is the area A times the stress, or $F = A\sigma = AE\left(\frac{\partial u}{\partial x}\right)$. The particle velocity and acceleration can be calculated by $\left(\frac{\partial u}{\partial t}\right)$ and $\left(\frac{\partial^2 u}{\partial t^2}\right)$, respectively, and the element mass a unit volume times the mass density $\rho$, $(Adx)\rho$.

Now applying Newton's Second law:

$$\sum F_x = \sum ma_x \qquad \text{Eq. (2.5.1)}$$

to the an element on the bar with tensile stresses chosen as positive yields:

$$AE\left[\frac{\partial u}{\partial x} + \frac{\partial}{\partial x}\left(\frac{\partial u}{\partial x}\right)dx\right] - AE\frac{\partial u}{\partial x} = (Adx)\rho\frac{\partial^2 u}{\partial t^2} \qquad \text{Eq. (2.5.2)}$$

Solving gives:

$$\frac{\partial^2 u}{\partial t^2} = \frac{E}{\rho}\frac{\partial^2 u}{\partial x^2} = c^2\frac{\partial^2 u}{\partial x^2} \qquad \text{Eq. (2.5.3)}$$

where: $c = \sqrt{E/\rho}$.

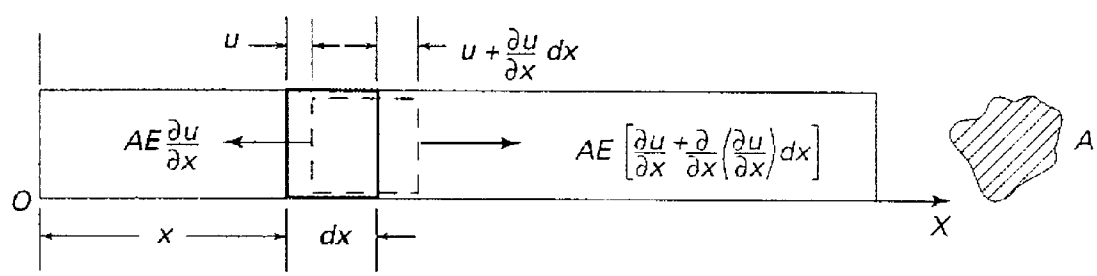


**Figure 2.5.1** - Forces and displacements on an element of an elastic bar.

The general solution of the partial differential equation (2.5.3) is $u = f(x - ct) + f'(x + ct)$ which can be verified by substitution back into equation (2.5.3). The particular functions $f$ and $f'$ remain to be evaluated. The parameters $(x - ct)$ and $(x + ct)$ indicated that the displacement and its derivatives, strain and velocity, travel through the bar in waves. The value of the function at a point $x$ and a time $t$ moves unchanged for an increment of time $\Delta t$ to a new position $(x + \Delta x)$, where $\Delta x$ is an amount such that the value of the parameter remains unchanged. See Figure 2.5.2.

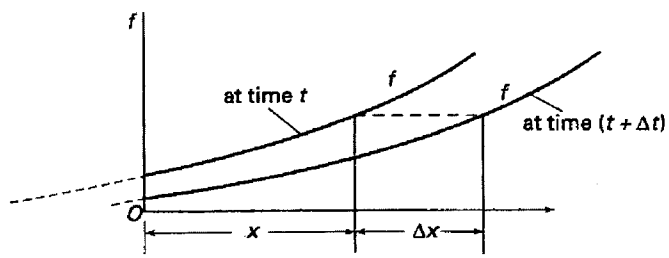


**Figure 2.5.2** - Travel of $\Delta x$ of the value function $f$ in time increment $\Delta t$.

So for the parameter of function $f$, $(x + \Delta x) - c(t + \Delta t) = x - ct$, where $\Delta x = c\Delta t$. The velocity of the function is $\frac{\Delta x}{\Delta t} = c = \sqrt{E/\rho}$, which is commonly called the speed of sound for the given material and is much greater than the velocity $\frac{\partial u}{\partial t}$ of the particles, which has very small relative displacements.

It can now be seen that the wave for the function $f$ has a positive velocity and that it moves continuously to the right. Likewise, the parameter of the function $f'$ indicates that its wave velocity is $\frac{\Delta x}{\Delta t} = -c$, a negative velocity or continuous motion to the left. The displacement $u$ is the sum of a function in a positive wave and the displacement in a negative wave, and so are its derivatives.

The relationship between stress and particle velocity needs to be established. For the positive portion of the wave, designate the function $f$ as $y$, the stress as $s$, and the velocity as $v$. Then $y = x - ct$, and

$$v = \frac{\partial f}{\partial t} = \frac{\partial f}{\partial y}\frac{\partial y}{\partial t} = \frac{\partial f}{\partial y}(-c) \qquad \text{Eq. (2.5.4)}$$

and

$$s = E\frac{\partial f}{\partial x} = E\frac{\partial f}{\partial y}\frac{\partial y}{\partial x} = E\frac{\partial f}{\partial y}(1) \qquad \text{Eq. (2.5.5)}$$

Their ratio is

$$\frac{v}{s} = \frac{-c}{E} = \frac{-\sqrt{E/\rho}}{E} = -\frac{1}{\sqrt{E\rho}} \qquad \text{Eq. (2.5.6)}$$

so,

$$v = -\frac{s}{\sqrt{E\rho}} \quad \text{and} \quad s = -v\sqrt{E\rho} \qquad \text{Eq. (2.5.7a \& b)}$$

From these equations it can be seen that in a positive wave, one that propagates to the right, particles that move with a positive velocity $v$ give a negative value of stress (compression). Likewise, particles moving in a negative direction give a positive value of stress (tension). See Figure 2.5.3a.

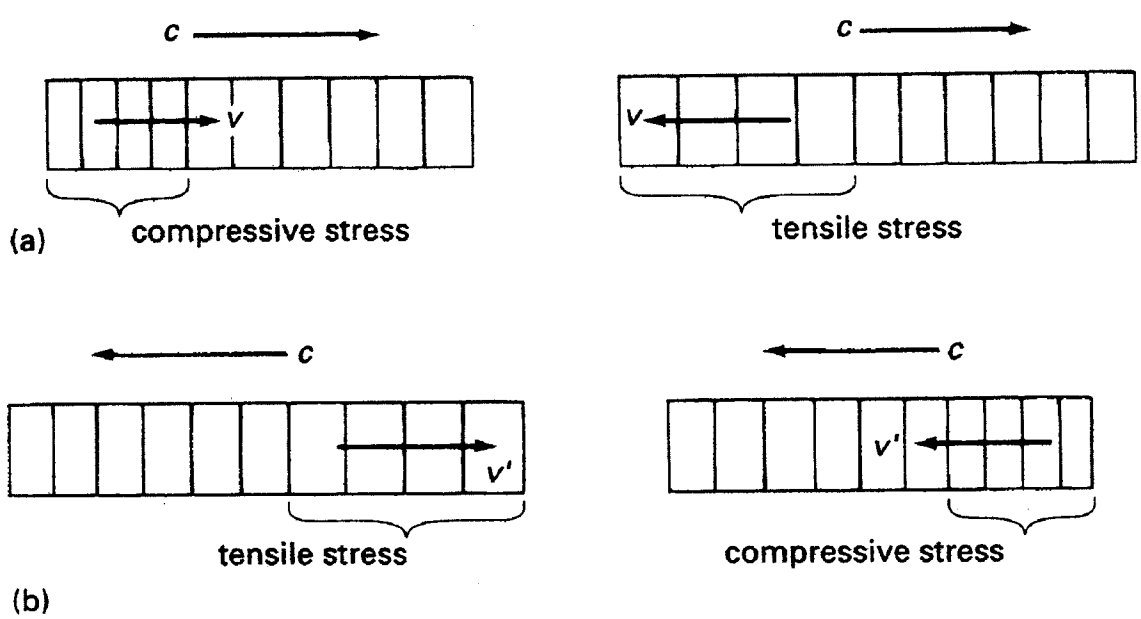


**Figure 2.5.3** - Strains and corresponding stresses in (a) a positive wave - propagating to the right; (b) a negative wave - propagating to the left.

For a negative wave, designate the function $f'$ as $z$, the stress as $s'$, and the velocity as $v'$. Then, $z = x + ct$, and

$$v' = \frac{\partial f'}{\partial t} = \frac{\partial f'}{\partial z}\frac{\partial z}{\partial t} = \frac{\partial f'}{\partial z}(+c) \qquad \text{Eq. (2.5.8)}$$

and

$$s' = E\frac{\partial f'}{\partial x} = E\frac{\partial f'}{\partial z}\frac{\partial z}{\partial x} = E\frac{\partial f'}{\partial z}(1) \qquad \text{Eq. (2.5.9)}$$

Their ratio is

$$\frac{v'}{s'} = \frac{c}{E} = \frac{\sqrt{E/\rho}}{E} = \frac{1}{\sqrt{E\rho}} \qquad \text{Eq. (2.5.10)}$$

so,

$$v' = \frac{s'}{\sqrt{E\rho}} \quad \text{and} \quad s' = v'\sqrt{E\rho} \qquad \text{Eq. (2.5.11a \& b)}$$

Thus from these equations it can be seen that in a negative wave positive particle velocities give positive stresses (tension) and negative particle velocities give negative stresses (compression). See Figure 2.5.3b.

The total stress $\sigma$ is the sum of the stresses in these two waves,

$$\sigma = E\frac{\partial u}{\partial x} = E\left(\frac{\partial f}{\partial x} + \frac{\partial f'}{\partial x}\right) = s + s' \qquad \text{Eq. (2.5.12)}$$

Likewise, the net velocity $V$, in terms of stresses, is

$$V = \frac{\partial u}{\partial t} = \frac{\partial f}{\partial t} + \frac{\partial f'}{\partial t} = v + v' = \frac{1}{\sqrt{E/\rho}}(-s + s') \qquad \text{Eq. (2.5.13)}$$

Thus, if the wave-stress distributions $s$ and $s'$ at any time $t$ are known, they can be added to obtain the total stress and subtracted to find the net particle velocity.

It should be clear that finding the particular functions $f$ and $f'$; which is no easy task, especially for complex geometries, is the key to applying this method. Even if the particular functions are known, solving the

partial differential field equations themselves is by no means a trivial task. Although this method can give exacting results, the validity of the equations is still limited to the elastic region. It is for these reasons that the simplifications and assumptions used in the energy method are usually employed.

## 2.6 The Theoretical Basis of Event Simulation[4]

Event simulation, as an engineering methodology, is vastly different from the techniques that have been taught to engineers since the onset of formal engineering training. Event simulation is actually virtual engineering where a physical event is simulated in a virtual laboratory. Performing an engineering analysis using event simulation requires a slightly different viewpoint from that of a classical stress analysis. The remainder of this section will more clearly define event simulation and contrast it with classical stress analysis.

In engineering school, it is taught that stress is a function of force, or $\sigma = f(\text{force})$, and that the deformation, or displacement, is another function of force, or $\delta = g(\text{force})$. In virtual engineering, however, it is assumed that the design force is indeterminate and results from some type of outside action or motion. In this scenario, force and stress are functions of displacement or deformation; that is $\sigma = f(\delta)$ and force $= g(\delta)$. The deformation is calculated directly from the governing physical equations.

A simple cantilever beam, like used in this study, is used to demonstrate the basic differences between classical stress analysis and event simulation.

---

[4] Taken from "The Theoretical Basis of Event Simulation" by Algor, Inc.

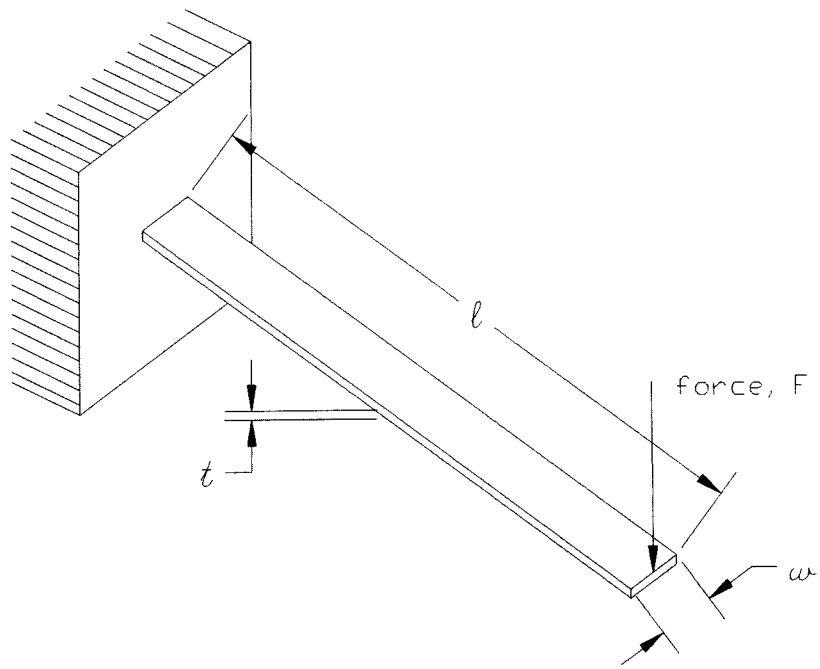


**Figure 2.6.1** - Typical cantilever beam with a load F on the free end.

Using the standard engineering formula for a cantilever beam in flexure due to force at the free end, the maximum stress at the wall (fixed support) is given by:

$$\sigma = \frac{Mc}{I} \qquad \text{Eq. (2.6.1)}$$

where:

M is the moment generated by the force F: $M = Fl$

l is the length of the beam from the force to the wall

c is the distance from the neutral axis to the outer fibers: $c = \frac{t}{2}$

t is the thickness of the beam

I is the area moment of inertia of the cross section: $I = \frac{wt^3}{12}$

w is the width of the beam.

This result is obtained by considering the pure bending of a beam in conjunction with Hooke's law:

$$|F| = k|\delta| \qquad \text{Eq. (2.6.2)}$$

This law states that force is a linear function of displacement, which forms the basis of classical stress analysis and modern finite element stress analysis.

In finite element analysis, the matrix equation $\{\mathbf{F}\} = [\mathbf{K}]\{\delta\}$ is solved for the displacement vector, $\{\delta\}$, from the force vector, $\{\mathbf{F}\}$, and the stiffness matrix, $[\mathbf{K}]$. Subsequently, the stresses are calculated from Hooke's law by the equation $\{\sigma\} = E\{\varepsilon\}$, where $\{\varepsilon\}$ is the strain vector, which is the normalized displacement vector and E is Young's modulus, which is related to Hooke's constant, k, by $E = \frac{k}{\delta}$ .

No further investigation would be required if the beam were always in static equilibrium and within the elastic deflection region, which is the only valid application of equation (2.6.1). In practical mechanical engineering, the static case almost never dictates the design criteria. The design must consider the "worst case scenario," which would generally occur when the beam is in motion and the forces, and thus the stresses, are greater than those predicted under static conditions.

Now virtual engineering enters the design process: it allows the simulation of an entire event, not simply a static condition. Since the assumption is that the beam is no longer static, a dynamic approach is taken. The force that the beam is subjected to are now considered to be generated by its motion. Now consider the relationship between motion and force.

According to Newton's second law, force equals mass multiplied by acceleration.

$$F = ma \qquad \text{Eq. (2.6.3)}$$

Mass is an inherent property of all matter, and acceleration is simply the time rate of change of velocity, $a = \frac{dv}{dt}$. This law quantifies the fact that mass is the property of matter that causes resistance to changes in motion. It should also be noted that under the influence of gravity, the special case of constant acceleration, a body at rest of mass m generates a force, its weight, of mg, where g is the acceleration due to gravity. For a differential time *dt*, equation (2.6.2) can be arranged into the impulse-momentum equation.

$$dF = m\frac{dv}{dt} \quad \text{or} \quad dFdt = mdv \qquad \text{Eq. (2.6.4)}$$

For a finite time increment of Δt, equation (2.6.3) becomes:

$$F = m\frac{\Delta v}{\Delta t} \quad \text{or} \quad F\Delta t = m\Delta v \qquad \text{Eq. (2.6.5)}$$

where Δv is the average change in velocity over the time increment, Δt. From this relationship, a 1,000 lb. force acting over a Δt of 0.001 sec. produces the same net impulse as a 1 lb. force acting over a Δt of 1 sec.

Event simulation is based on the combination of Newton's second law with Hooke's law as follows by combining equations (2.6.2) and (2.6.3) to give:

$$F = ma = -k\delta \quad \text{or} \quad ma + k\delta = 0 \qquad \text{Eq. (2.6.6)}$$

The negative sign in front of k is due to the displacement opposing the direction of the force. Also, note that the quantity (variable) force F can be eliminated, and that the concept of time has been introduced through the acceleration. In order to simulate real world problems, various damping and friction factors must also be taken into account. Such dissipative forces can be modeled by:

$$F = -cv \qquad \text{Eq. (2.6.7)}$$

where v is the velocity and c is a general damping constant. Note that the dissipation also opposes the motion (force). Combining equations ((2.4.2), (2.6.3) and (2.6.7) yields:

$$F = ma = -k\delta = -cv \quad \text{or} \quad ma + k\delta + cv = 0 \qquad \text{Eq. (2.6.8)}$$

or in a more computer usable matrix form:

$$[\mathbf{m}]\{\mathbf{a}\} + [\mathbf{c}]\{\mathbf{v}\} + [\mathbf{K}]\{\delta\} = 0 \qquad \text{Eq. (2.6.9)}$$

This is the basic equation of virtual engineering. Note how it models a dynamic system in the same manner as in a vibrations analysis problem instead of using the classical strength of materials methods. The combination of motion, damping and mechanical deformation can be applied to any structure since all materials have some degree of elasticity, and therefore can be modeled as a classical mass-spring-damper system according to the equation $m\ddot{x} + c\dot{x} + kx = F(t)$. See Figure 2.6.2.

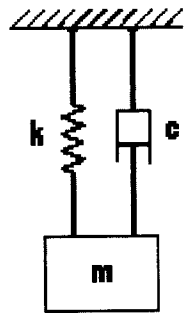


**Figure 2.6.2** - Diagram representing a typical spring-mass-damper system

Since the stresses are still typically of interest, they can be calculated at any time during the analysis by application of Hooke's law, $\{\sigma\} = E\{\varepsilon\}$, where the strain vector, $\{\varepsilon\}$, is easily obtained from the displacement vector $\{\delta\}$. Event simulation provides a means by which to design for the "worst case scenario." Even for the relatively simple example of the cantilever beam, the solution of equation (2.6.9) is beyond the realm of hand calculation but, today's computer technology has reduced the solution of significantly more complex problems to a more practical level.

Event simulation allows one to model an entire physical event with the least number of assumptions. Specifically, one does not have to assume a static situation or have to estimate values for forces that result from motion. Furthermore, event simulation supplies, as a useful byproduct, a "frame-by-frame" record of the event, not just a single "snap-shot" at its conclusion.

# Chapter 3: Experimental Material Testing

Experimental material testing was performed on three samples of the material used in the experimental stress analysis portion of this research project to determine property values. The specific values for Young's Modulus (E) and the post yield strain hardening tangent modulus ($E_t$) were needed for the computational software.

The material used was believed to be 2024-T6 aluminum. However, since there was an uncertainty in the material and there are slight variations of material properties among different heats of the same material, tensile tests were conducted to obtain the values of E and $E_t$. These values for the three tests were averaged and used as the accepted values the software.

The tensile samples were machined from test bars from the same box as those used in the experimental portion of this study according to the 1980 Annual Book of ASTM Standards Part 10: Metals - Physical, Mechanical, Corrosion Testing. Figure 3.1 shows the geometry of the specimens.

The tests were performed at Satec Systems, Inc. in Grove City, PA using a SATEC EMF 33 tensile testing machine interfaced to a personal computer equipped with a data acquisition card and Satec's tensile testing software. See appendix A for the machine's certification sheet.

The three tests were run at a controlled rate of stressing of 50,000 psi/min. The average value obtained for E was $9.87\times10^6$ psi, $\sigma_{yield}$ was $\approx$47,167 psi, and $E_t$ was $1.08 \times 10^6$ psi. Table 3.1 shows the physical dimensions of the individual test specimens and Table 3.2 shows a summary of the values obtained from the three tests and compares them to values listed

by the Aluminum Association. Figures 3.2, 3.3, and 3.4 show the graphical output obtained from the PC controlled testing machine.

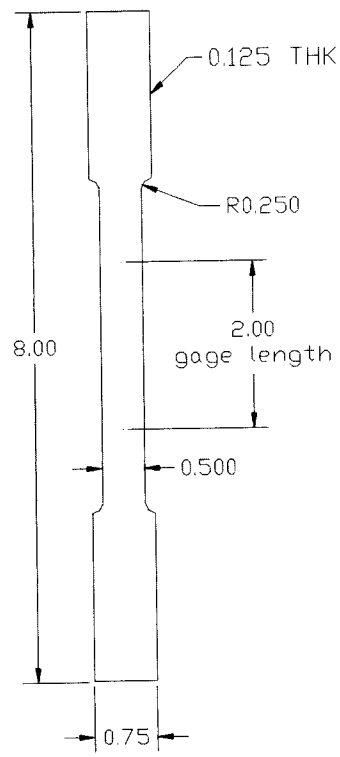


**Figure 3.1** - Drawing of tensile specimen for sheet material as specified by 1980 Annual Book of ASTM Standards Part 10: Metals - Physical, Mechanical, Corrosion Testing

| | Gage width (in) | Gage thickness (in) | Pretest gage length (in) | Posttest gage length (in) |
|---|---|---|---|---|
| **Specimen #1** | 0.5000 | 0.1220 | 2.000 | 2.366 |
| **Specimen #2** | 0.5000 | 0.1230* | 2.000 | 2.32 |
| **Specimen #3** | 0.5000 | 0.1220 | 2.000 | 2.335 |
| **Average** | 0.5000 | 0.1223 | 2.000 | 2.340 |

**Table 3.1** - Physical dimensions of the test specimens.

* Specimen #2 broke just outside the prescribed gage length, therefore some values for this sample may be slightly in error.

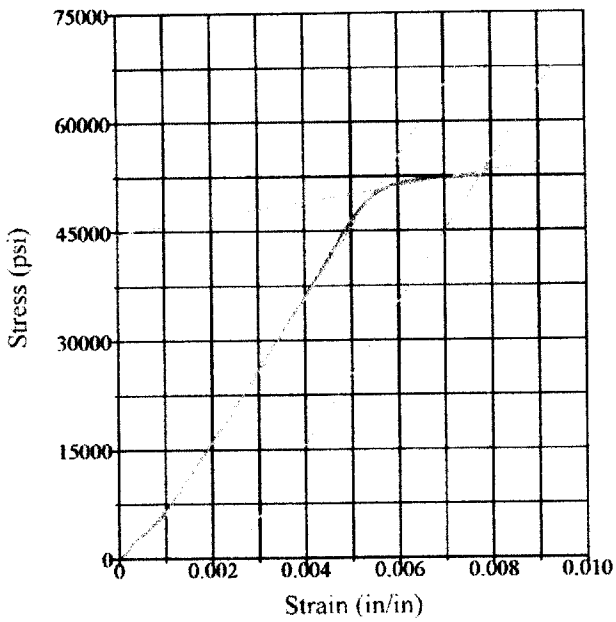


**Test Results**

| | |
|---|---|
| Width: | **0.5000** in |
| Thickness: | **0.1220** in |
| Area: | **0.0610** in² |
| Tangent Modulus: | **9800420** psi |
| Stress at Offset: | **52430** psi |
| Tensile Strength: | **69570.4900** psi |
| Stress at Break: | **15630** psi |
| Peak Load: | **4243.8000** lbf |
| Total Elongation: | **18.3000** % |
| Pretest Punch Length: | **2** in |
| Posttest Punch Length: | **2.366** in |
| Tangent Modulus#2: | **1070620** psi |

**Test Summary**

| | |
|---|---|
| Counter: | **122** |
| Elapsed Time: | **00:01:54** |
| Specimen Identification: | **1** |
| Procedure Name: | **All Purpose Tensile** |
| Start Date: | **7/9/98** |
| Start Time: | **2:15:56 PM** |
| End Date: | **7/9/98** |
| End Time: | **2:17:50 PM** |
| Workstation: | **SATEC** |

**Figure 3.2** - Sample 1. Stress vs. strain curve output from SATEC Systems, Inc. tensile test machine and software interface.

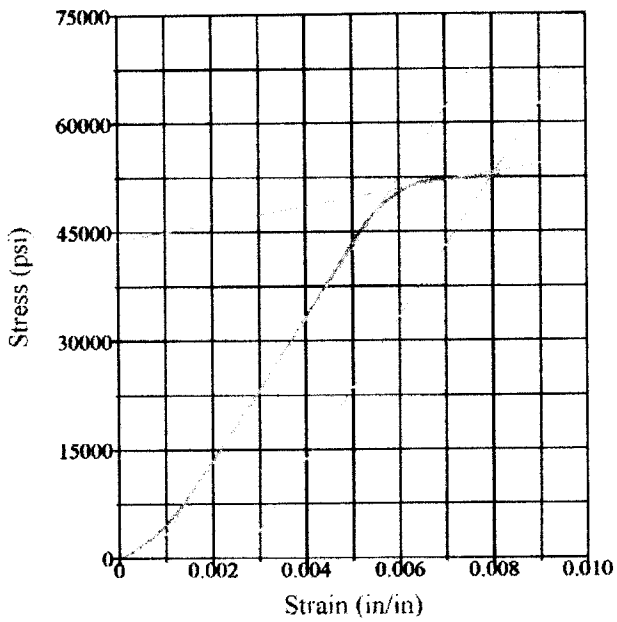


**Test Results**

| | |
|---|---|
| Width: | **0.5000** in |
| Thickness: | **0.1230** in |
| Area: | **0.0615** $in^2$ |
| Tangent Modulus: | **9786060** psi |
| Stress at Offset: | **52580** psi |
| Tensile Strength: | **71269.9200** psi |
| Stress at Break: | **22930** psi |
| Peak Load: | **4383.1000** lbf |
| Total Elongation: | **16.0000** % |
| Pretest Punch Length: | **2** in |
| Posttest Punch Length: | **2.32** in |
| Tangent Modulus#2: | **1178730** psi |

**Test Summary**

| | |
|---|---|
| Counter: | **123** |
| Elapsed Time: | **00:02:02** |
| Specimen Identification: | **2** |
| Procedure Name: | **All Purpose Tensile** |
| Start Date: | **7/9/98** |
| Start Time: | **2:32:13 PM** |
| End Date: | **7/9/98** |
| End Time: | **2:34:15 PM** |
| Workstation: | **SATEC** |

**Figure 3.3** - Sample 2. Stress vs. strain curve output from SATEC Systems, Inc. tensile test machine and software interface.

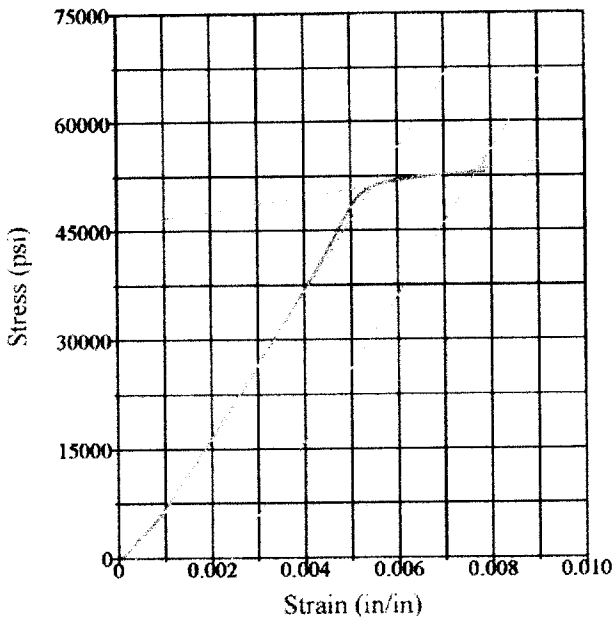


**Test Results**

| | |
|---|---|
| Width: | **0.5000** in |
| Thickness: | **0.1220** in |
| Area: | **0.0610** $in^2$ |
| Tangent Modulus: | **10013600** psi |
| Stress at Offset: | **52910** psi |
| Tensile Strength: | **71136.0700** psi |
| Stress at Break: | **15800** psi |
| Peak Load: | **4339.3000** lbf |
| Total Elongation: | **16.7500** % |
| Pretest Punch Length: | **2** in |
| Posttest Punch Length: | **2.335** in |
| Tangent Modulus#2: | **1007080** psi |

**Test Summary**

| | |
|---|---|
| Counter: | **124** |
| Elapsed Time: | **00:01:58** |
| Procedure Name: | **All Purpose Tensile** |
| Start Date: | **7/9/98** |
| Start Time: | **2:42:14 PM** |
| End Date: | **7/9/98** |
| End Time: | **2:44:12 PM** |
| Workstation: | **SATEC** |
| Specimen Identification: | **3** |

**Figure 3.4** - Sample 3. Stress vs. strain curve output from SATEC Systems, Inc. tensile test machine and software interface.

| | Specimen # 1 | Specimen # 2 | Specimen # 3 | Average | Standard Accepted Values* | % Difference |
|---|---|---|---|---|---|---|
| **Young's Mod. (E) (psi)** | 9,800,420 | 9,786,060 | 10,013,600 | **9,866,693** | **10,600,000** | **6.92** |
| **Tangent Mod. ($E_t$) (psi)** | 1,070,620 | 1,178,730 | 1,007,080 | **1,085,477** | **N/A** | **-** |
| **Yield Stress (psi)** | ≈ 47,000 | ≈ 47,500 | ≈ 47,000 | **47,167** | **47,000** | **0.36** |
| **Tensile Strength (psi)** | 69,570 | 71,270 | 71,136 | **70,659** | **68,000** | **3.76** |
| **Pretest Gage Length (in)** | 2.00 | 2.00 | 2.00 | **2.00** | **2.00** | **-** |
| **Posttest Gage Length (in)** | 2.366 | 2.32+ | 2.335 | 2.3403 | **-** | **-** |
| **% Elongation** | 18.3 | 16.0 | 16.75 | 17.01 | **20** | **14.9** |

**Table 3.2** - Results of tensile tests.

**NOTE:** These tests were run at a constant rate of stress of 50,000 psi/min.

* These values are as published by the Aluminum Association in the 1979 aluminum standards and data book. Values were obtained from a 1/16 in. thick sample and not a 1/8 in sample as was used in this testing.

+ Specimen # 2 broke outside of the prescribed gage length and therefore values for the posttest gage length and percent elongation my be in err.

# Chapter 4: Finite Element Analysis / Event Simulation

The finite element analysis (FEA) performed in this study was a nonlinear event simulation. The nonlinear software had to be employed to predict the yielding that occurred due to the severity of the impact loading. The modeling of the impact event served two functions. The first purpose was to determine the accuracy with which the outcome of the event could be predicted. Secondly, the strain results of the FEA model were used as a guide to set the bounding limits of the data acquisition unit used to capture dynamic strain readings during the actual laboratory impact tests.

The FEA model was built using two material groups. The first group (shown in green) was used to model the aluminum test beam and the second group (shown in gold) was used to simulate the falling mass. See Figure 4.1.

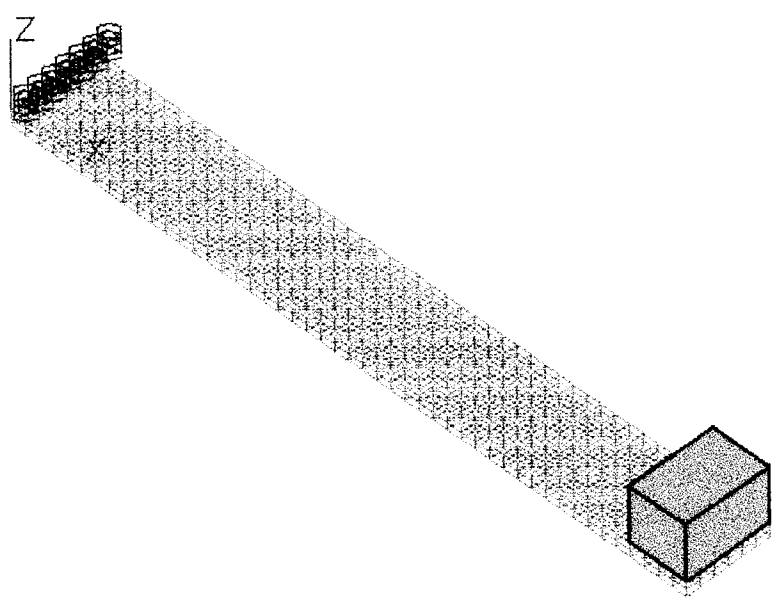


**Figure 4.1** - The FEA model used to simulate the impact of a free falling mass. The aluminum beam is shown in green, the full constraint boundary conditions are in red, and the impacting mass is shown in gold.

The aluminum test beam (group 1 in the model) was constructed to the physical dimensions of the experimental test beams. The group 1 model was six inches long, three-fourths of an inch wide, and one-eighth of an inch thick. Since the beam was the critical area of interest, this portion of the model was constructed of 576 $\frac{1}{8} \times \frac{1}{8} \times \frac{1}{16}$ inch 20 node brick elements for a total of 3605 nodes. See Figures 4.2 and 4.3. The 20 node brick configuration allows more iteration points within the model for improved accuracy, however, the increased number of nodes also increases the run time required for a solution. The final configuration of this simple nonlinear model nearly exceeded the capacity of the computer used. For this reason, the model was built with the relatively large $\frac{1}{8} \times \frac{1}{8}$ inch surfaces, and two bricks deep for improved accuracy through the thickness. Ideally, at minimum, perfect $\frac{1}{32}$ inch cube elements would be used. This should provide greater accuracy on the outer surfaces and give four elements to better distribute the stresses through the thickness and show any shift in the neutral axis due to plasticity.

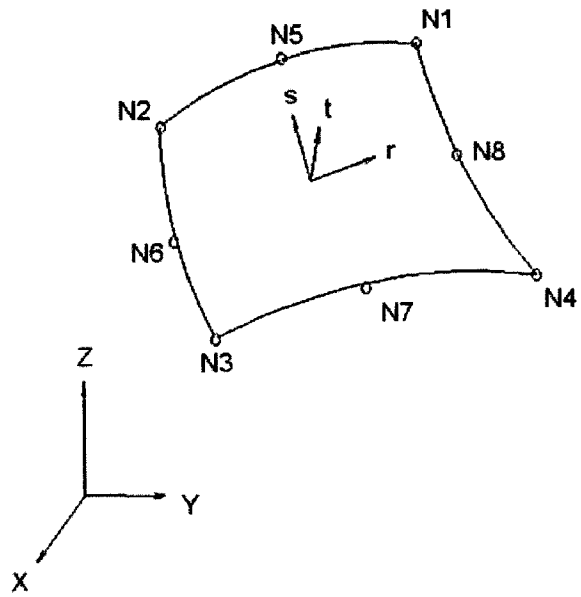


**Figure 4.2** - The basic formulation of a 3-D element. Note the node numbering and the local coordinate systems. The 20 node brick is formed by extruding this figure into its third dimension.

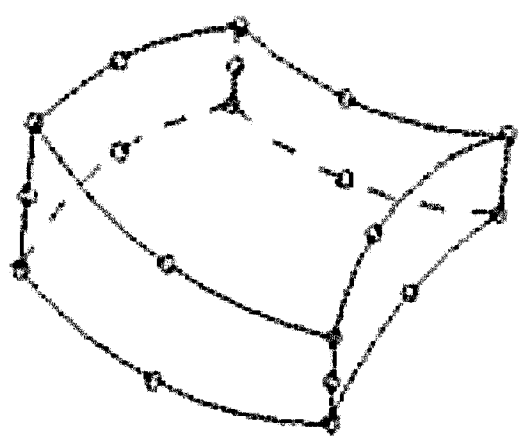

**Figure 4.3** - The basic formulation of a 20 node brick.

The element type used was the Von Mises yield criteria with isotropic hardening. A fourth order integration in the *r-s* plane and in the *t* direction was also used for improved accuracy. Refer back to Figure 4.2. The

isotropic hardening model involves a uniform increase of the yield surface due to work hardening. Isotropic hardening applies mainly to monotonic loading, without stress reversals, such as the one time impact this model experienced. The material properties of E, $E_t$, $\nu$, $\sigma_{yield}$, and $\rho$ for the aluminum beam required by the Von Mises assumption were assigned in the decoder. Note that E is Young's modulus, $E_t$ is the strain hardening modulus, $\nu$ is Poisson's ratio, $\sigma_{yield}$ is the yield stress in simple tension. These values were obtained from the tensile tests performed in Chapter 3. The variable $\rho$ is the mass density of the material. This value was obtained by dividing the weight density of aluminum by the gravitational constant, $g_c$.

The impacting mass (group 2) was modeled as a single eight node brick and given an equivalent mass density to equal 6.25 lbs., the same as the lead weight used in the laboratory experiment, when subjected to gravity. The mass was also given an initial velocity of $V_o = \sqrt{2gh} = \sqrt{2(386.4\,{}^{in}/_{sec^2})(2in)} = 39.31\,{}^{in}/_{sec}$ to eliminate the computer run time required to iterate through the time steps for the free fall. Since the impacting mass was not a focal point, a three dimensional linearly elastic element type was chosen with only a second order integration in the *r-s* plane and in the *t* direction. The appropriate values of E, $\nu$, and $\rho$ were again entered into the decoder to describe the physical characteristics of the pseudo material used to simulate the impacting mass. Refer to Appendix B for a complete list of the Algor Decoder options selected.

The model was run with initial impact occurring at time t = 0 sec. The maximum longitudinal strain occurred at time t = 0.0505 sec. at the cantilevered end, as was expected, indicating that plastic deformation was present. The output from this time step verified that at the location of gage #1

(near the cantilever) plastic deformation would occur and at gage #2 (the center of the beam) all deformation was contained within the elastic region. Figures 4.4, 4.5, 4.6, 4.7, and 4.8 show the displacements of five time steps from initial impact to the maximum deflection of the undamped model. Note that in Figures 4.4 - 4.8 the impacting mass has been masked from the picture to emphasize the deflection of the beam. Table 4.1 shows the maximum strains predicted at the location of the two strain gages for a model with no damping and a model with a "moderate" Rayleigh damping factor of $\alpha = 2.5$ and $\beta = 0.5$. The total Rayleigh damping is $C = \alpha[M] + \beta[K]$ where $[M]$ is the mass matrix and $[K]$ is the stiffness matrix of the system.

Figures 4.9 and 4.10 are isometric views of the undamped model which show the flexural stress and longitudinal strain distribution over the top surface of the beam. Table 4.2 shows the maximum flexural stresses predicted at the location of the two strain gages for both models.

**Figure 4.4** - The initial impact at time t = 0. - No damping

**Figure 4.5** - Just after impact at time t = 0.0125 sec. - No damping

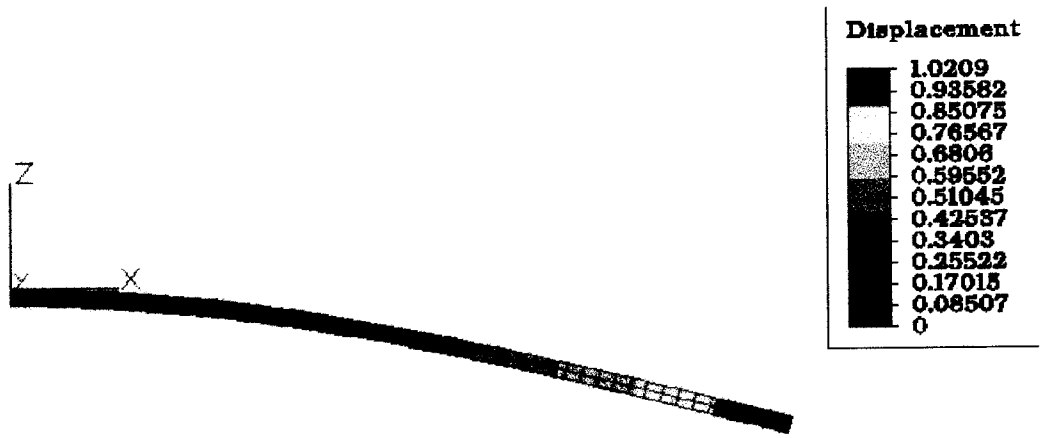


**Figure 4.6** - The displacement due to impact at time t = 0.025. - No damping

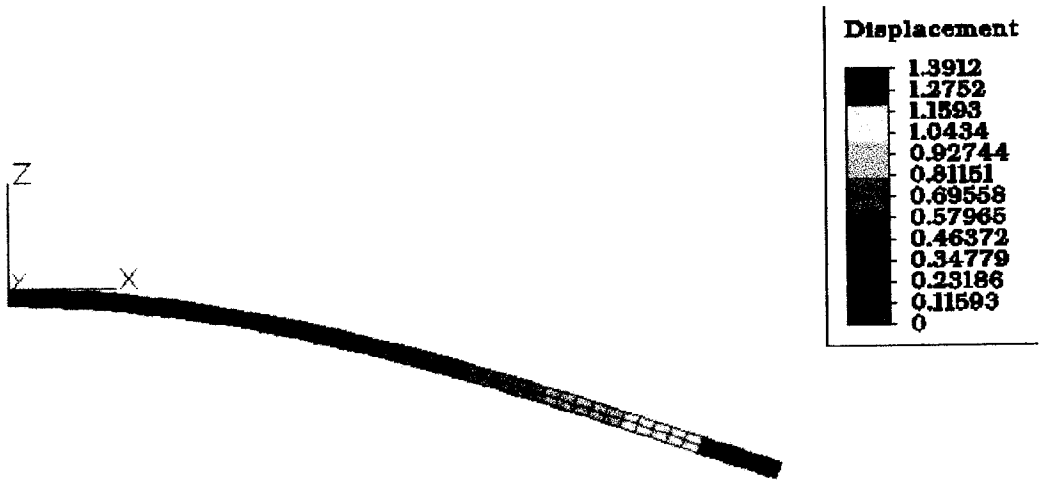


**Figure 4.7** - The displacement due to impact at time t = 0.0375 sec. - No damping

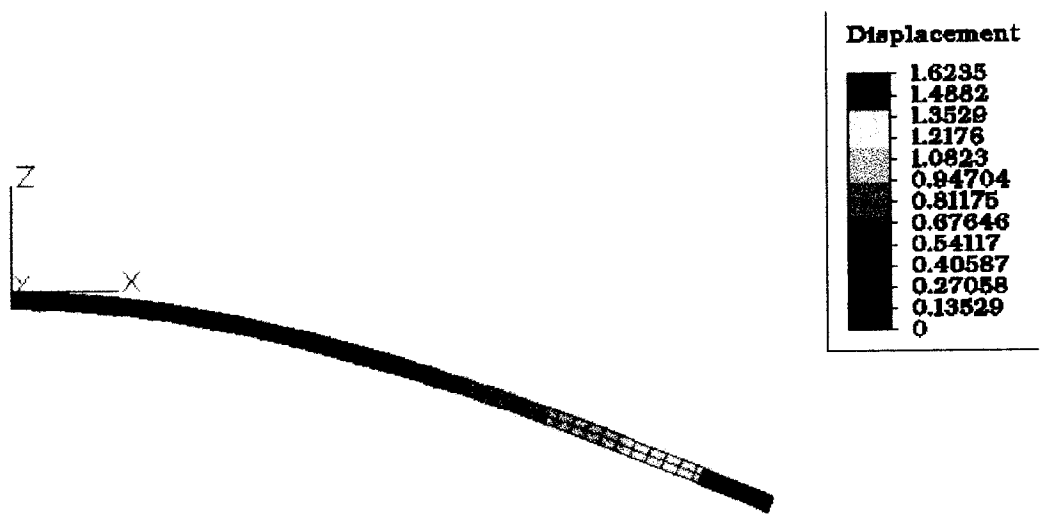


**Figure 4.8** - The point of maximum deflection. Time t = 0.0565 sec. - No damping

The following figures show the flexural stress and the longitudinal strain distributions over the top surface of the undamped model.

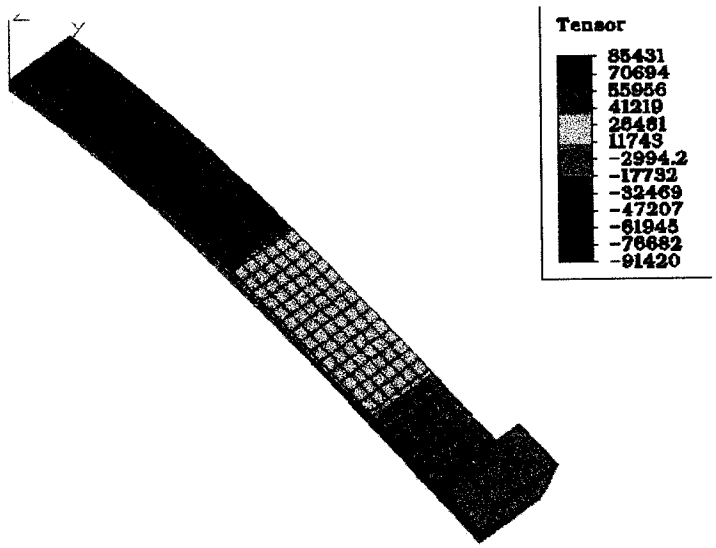


**Figure 4.9** - Isometric view of the flexural stress distribution over the top surface. - No damping.

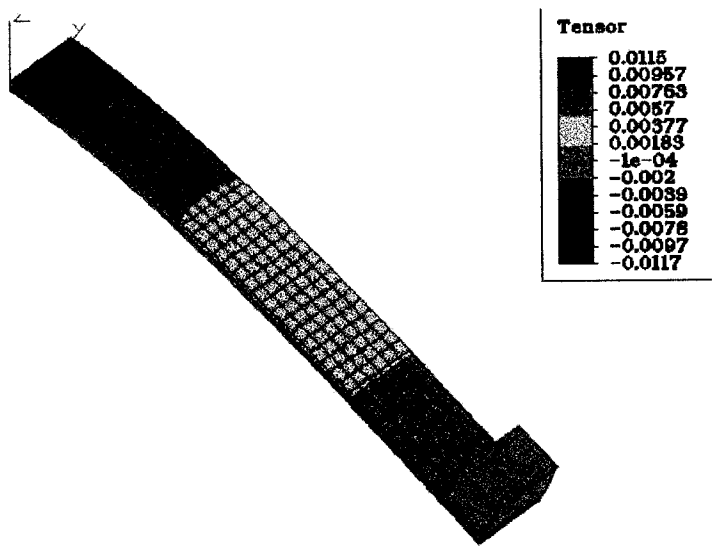


**Figure 4.10** - Isometric view of the longitudinal strain distribution over the top surface. No damping.

| | Peak Strains from FEA models | |
|---|---|---|
| | **No Damping** | **Damping w/ $\alpha = 2.5$, $\beta = 0.5$** |
| **Gage # 1 ( l = 5 in.)** | 7044 $\mu\varepsilon$ | 6242 $\mu\varepsilon$ |
| **Gage # 2 ( l = 3 in.)** | 3413 $\mu\varepsilon$ | 3190 $\mu\varepsilon$ |

**Table 4.1** - Maximum strain results at gage locations in FEA models.

| | Peak Flexural Stresses from FEA models | |
|---|---|---|
| | **No Damping** | **Damping w/ $\alpha = 2.5$, $\beta = 0.5$** |
| **Gage # 1 ( l = 5 in.)** | 50,185 psi | 50,918 psi |
| **Gage # 2 ( l = 3 in.)** | 30,998 psi | 29,425 psi |

**Table 4.2** - Maximum flexural stress results at gage locations in FEA models.

The results presented in Tables 4.1 and 4.2 are presented again in Chapter 6 as a comparison to the experimental portions of this work.

# Chapter 5: Experimental Verification

The purpose of the experimental work done in this study is to obtain actual values of the peak dynamic impact strain for the physical event that was simulated by the finite element analysis in the previous chapter. The values obtained by the experimentation are later used to judge the predictability and reliability of the event simulation software.

The experimental system was set up as shown in Figure 5.1. A personal computer and an SDA 2000 data acquisition unit were connected to the two strain indicators used to take the dynamic readings from strain gages mounted on the aluminum test beams. See Figures 5.2 and 5.3.

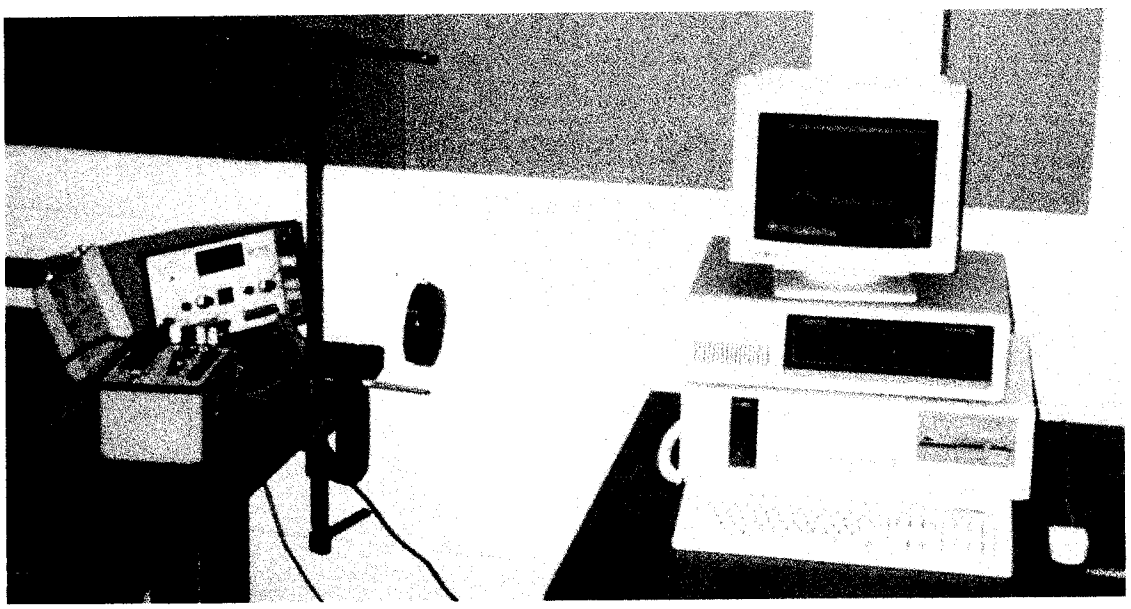

**Figure 5.1** - The experimental system set up.

**Figure 5.2** - Personal computer and SDA2000 data acquisition unit.

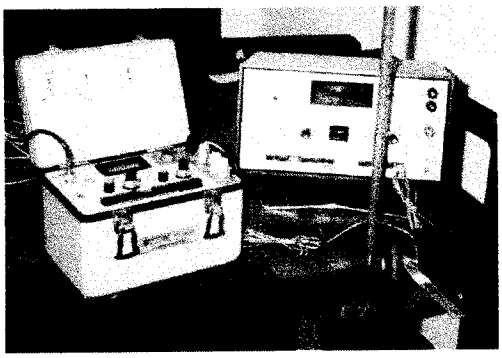

**Figure 5.3** - Strain indicators attached to test beam strain gages.

The item used as the impacting mass was a 6.25 lb. lead weight which was suspended two inches above the surface of the test beam with a thin piano wire, which was then cut with sharp side cutters to release the weight. Extra care was taken to ensure that the height was accurate and the weight was level in an attempt to obtain good square impacts with the end of the cantilever beam. The weight, 5 inches in diameter and $^{7}/_{8}$ inches thick, was positioned so the entire thickness of the weight struck the end of the cantilever beam with the edge of the weight and the end of the beam meeting flush. See Figure 5.4.

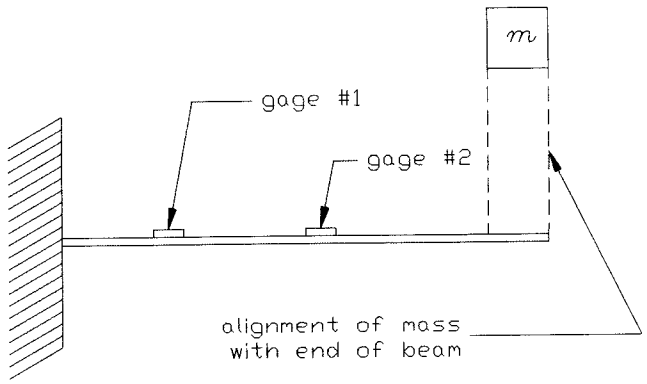


**Figure 5.4** - The weight aligned with the end of the cantilevered beam.

The test beams used were of the same material that the tensile specimens used to obtain the material properties. The electrical resistance strain gages used in the experiment were CEA-06-240UZ-120 universal general purpose static/dynamic gages from Micro-Measurements Division of Measurements Group, Inc. These gages are constructed of self temperature compensating Constantan foil, encapsulated in polyimide and have relatively large copper solder tabs for easy leadwire attachment.
See Figures 5.5 and 5.6.[1]

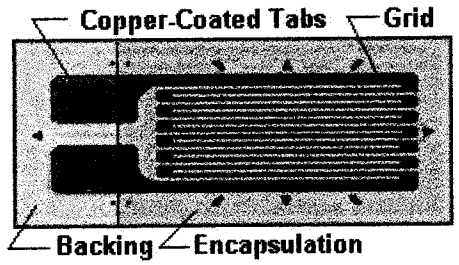


**Figure 5.5** - Typical CEA series gage showing the backing, copper tabs, encapsulation, and grid.

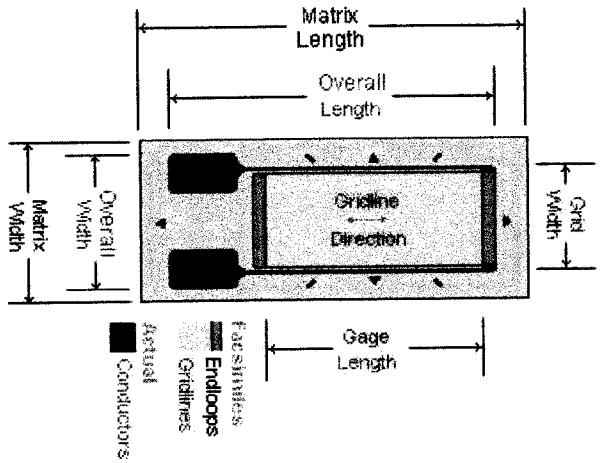


**Figure 5.6** - Nomenclature for a typical CEA series gage.

The gages used had an active gage length of 0.240 inches, which classified them as having a strain range of ±5% elongation or ±50,000 με, which was well above the projected 7000 - 8000 με range of the experiment. The gages were mounted, as specified in Vishay Measurements Group Education Division Bulletin 309D, using an M-Bond 200 cyanoacrylate kit. The M-Bond 200 adhesive is capable of an elongation of ±6% or ±60,000 με, again well above the projected range of the experiment. The leadwires were then soldered to the gages in a three wire circuit arrangement to eliminate any effects due to the resistance in the leadwires themselves. Each gage was the able to be connected to an individual strain indicator with an internal dummy gage to form a single active gage Wheatstone quarter bridge. See Figure 5.7.[1]

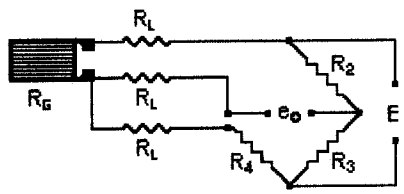


**Figure 5.7** - Diagram of a three wire circuit for a single active gage Wheatstone quarter bridge.

[1] Figures 5.5, 5.6, 5.7 were all obtained courtesy of http://www.measurementsgroup.com/

The beams were held to a massive laboratory table with a heavy duty 12 inch C-clamp to approximate a cantilevered connection. The individual gages were then connected to their respective strain indicators, and they in turn were connected to the data acquisition unit and the PC. Refer again to Figure 5.1.

Once the initial set up was complete, several false trials were run to set the limits on the data acquisition unit and ensure that the system would work as intended. Before the actual trials could be run, a relationship between the strain output of the strain indicators and the data recorded by the acquisition unit and PC. This was accomplished by two calibration techniques, to verify the same relationship. Since two strain gages were used, two recording channels were needed in the acquisition unit. The first channel recorded milli-volts (mV) and the second recorded milli-amperes (mA). Therefore, two conversion factors were needed to relate micro-strain (με) to milli-volts (mV) and milli-amperes (mA).

The first calibration method involved a known static load placed on the end of the cantilever beam and comparing the strain indicator readings with the millivolts recorded by the data acquisition unit. A 1.000kg mass was placed in the center of the beam 0.25 inches in from the free end. The strain indicators gave a strain reading of 565 με for gage #1 and 331 με for gage #2. A ratio of $^{\mu\varepsilon}/_{mV}$ and $^{\mu\varepsilon}/_{mA}$ could then be calculated. The data acquisition unit read 325 mA for gage #1 and 113 mV for gage #2. The conversion factor for gage #1 was $\left(\frac{565\mu\varepsilon}{325mA}\right) = 1.77\,{}^{\mu\varepsilon}/_{mA}$ and $\left(\frac{331\mu\varepsilon}{113mV}\right) = 2.93\,{}^{\mu\varepsilon}/_{mV}$ for gage #2.

The second calibration technique used the internal calibration shunt of each of the strain indicators. These produced a known calibration strain value

for each indicator which was again compared to the millivolts recorded by the data acquisition unit to arrive at the same ratios of $^{\mu\varepsilon}/_{mA} = 1.77$ for gage # 1 and $^{\mu\varepsilon}/_{mV} = 2.93$ for gage # 2 which were later used to convert the collected data into units of microstrain ($\mu\varepsilon$) to directly compare to the FEA results. See Figures 5.8 and 5.9 for graphical output of each method for a sample calibration step. These relationships remain linear through the entire active range of the strain gages, which is ±50,000 $\mu\varepsilon$, about seven times higher than the largest strain value recorded.

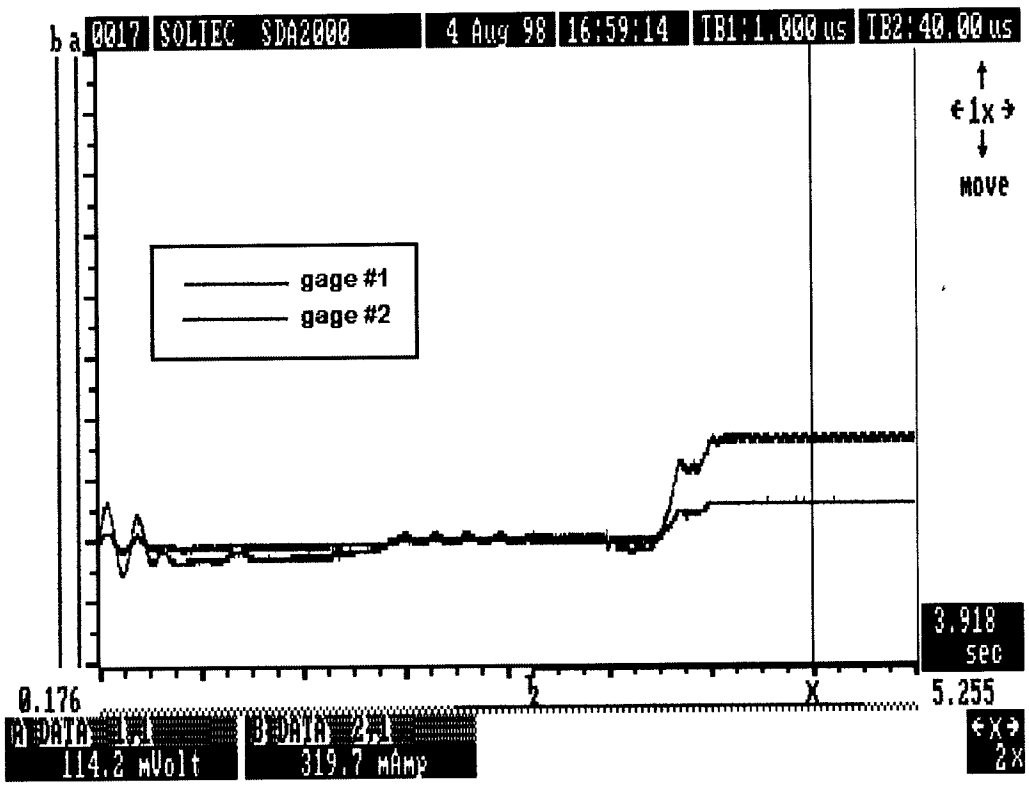


**Figure 5.8** - Graphical output of strain gage calibration using a static load

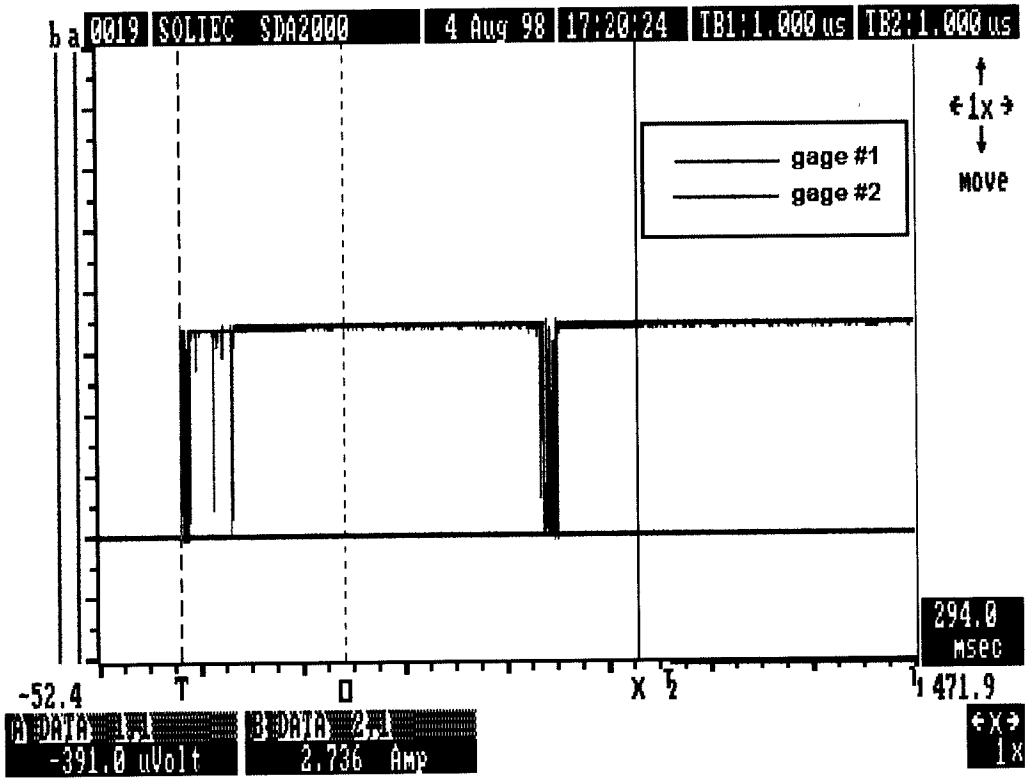


**Figure 5.9** - Graphical output of strain gage calibration using strain indicator internal shunt.

Three trials were run using the system described above. One trial failed to activate the data acquisition unit, however the permanent residual strain was able to be recorded from the strain indicator. The other two trials produced usable results captured by the data acquisition unit, with the second trial being used as the average of the experiment since it fell between the other two trials. Figure 5.10 shows the data captured from trial # 2 representing 524,288 samples per channel over 0.5243 seconds. Figure 5.11 shows the initial impact enlarged.

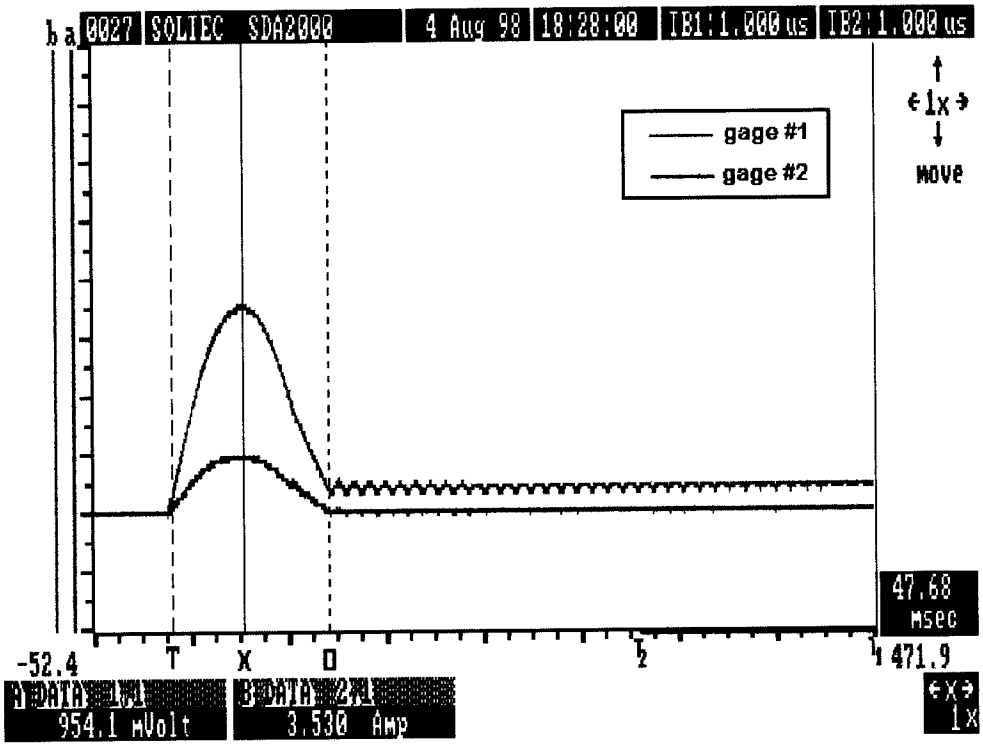


**Figure 5.10** - Trial # 2 captured data.

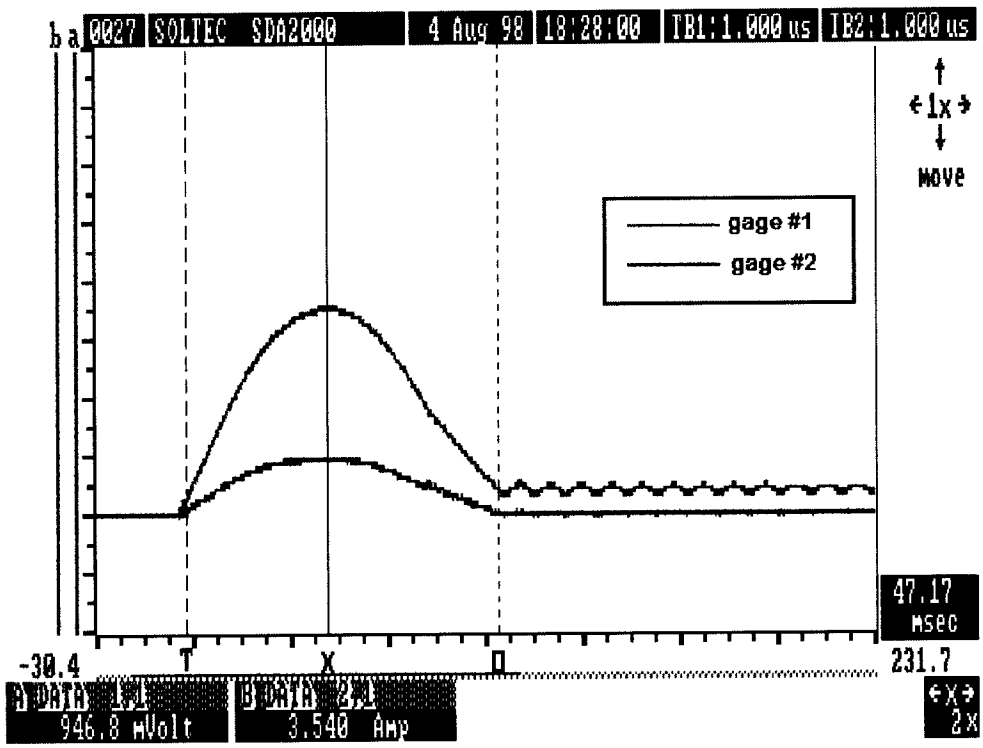


**Figure 5.11** - Trial # 2 captured data - initial impact enlarged.

Table 5.1 shows the collective results of the average experiment. The average of the experiment, assumed to be trial # 2, is later used as the accepted target in the comparison of the FEA models.

| | Peak Dynamic Strains from Experimental Trials | | |
|---|---|---|---|
| | Trial # 1 | Trial # 2 | Trial # 3* |
| Gage # 1 (l = 5 in.) | 5998 με | 6255 με | N/A |
| Residual Strain | 652 με | 720 με | 814 με |
| Gage # 2 (l = 3 in.) | 2678 με | 2817 με | N/A |
| Residual Strain | None | None | None |

**Table 5.1** - Maximum dynamic strain results at gage locations in the experimental trials.

* Trial # 3 was the trial which failed to activate the data acquisition unit. The residual strain was recorded from the strain indicator.

# Chapter 6: Results and Conclusions

## 6.1 Results

The results from the experimental impact and the FEA event simulation impact are presented and compared. The variation between the two sets of data is presented as a percentage difference from the experimental values. In this fashion the actual experimental strain values are considered to be the target value obtained by the software. Tables 6.1.1, 6.1.2, and 6.1.3 review the results of the FEA models and the experimental trials. Tables 6.1.4, 6.1.5, 6.1.6, and 6.1.7 directly compare the results of the FEA to the experimental data.

| | **Peak Strains from FEA models** | |
|---|---|---|
| | **No Damping** | **Damping w/ $\alpha = 2.5$, $\beta = 0.5$** |
| **Gage # 1 ( l = 5 in.)** | 7044 με | 6242 με |
| **Gage # 2 ( l = 3 in.)** | 3413 με | 3190 με |

**Table 6.1.1** - Maximum strain results at gage locations in FEA models.

| | **Peak Dynamic Strains from Experimental Trials** | |
|---|---|---|
| | **Trial # 1** | **Trial # 2*** |
| **Gage # 1 ( l = 5 in.)** | 5998 με | 6255 με |
| **Gage # 2 ( l = 3 in.)** | 2678 με | 2817 με |

**Table 6.1.2** - Maximum dynamic strain results at gage locations in the experimental trials.

* Trial # 2 is used as the mean for the experimental results since its values were bound by two other trials.

| | Peak Flexural Stresses from FEA models | |
|---|---|---|
| | **No Damping** | **Damping w/ $\alpha = 2.5$, $\beta = 0.5$** |
| **Gage # 1 ( l = 5 in.)** | 50,185 psi | 50,918 psi |
| **Gage # 2 ( l = 3 in.)** | 30,998 psi | 29,425 psi |

**Table 6.1.3** - Maximum flexural stress results at gage locations in FEA models.

A typical stress vs. strain curve from the Satec tests in Chapter 3 is used to compare values of stress predicted by the FEA directly to actual tensile data. See Figure 6.1.1 and Tables 6.1.5 and 6.1.6.

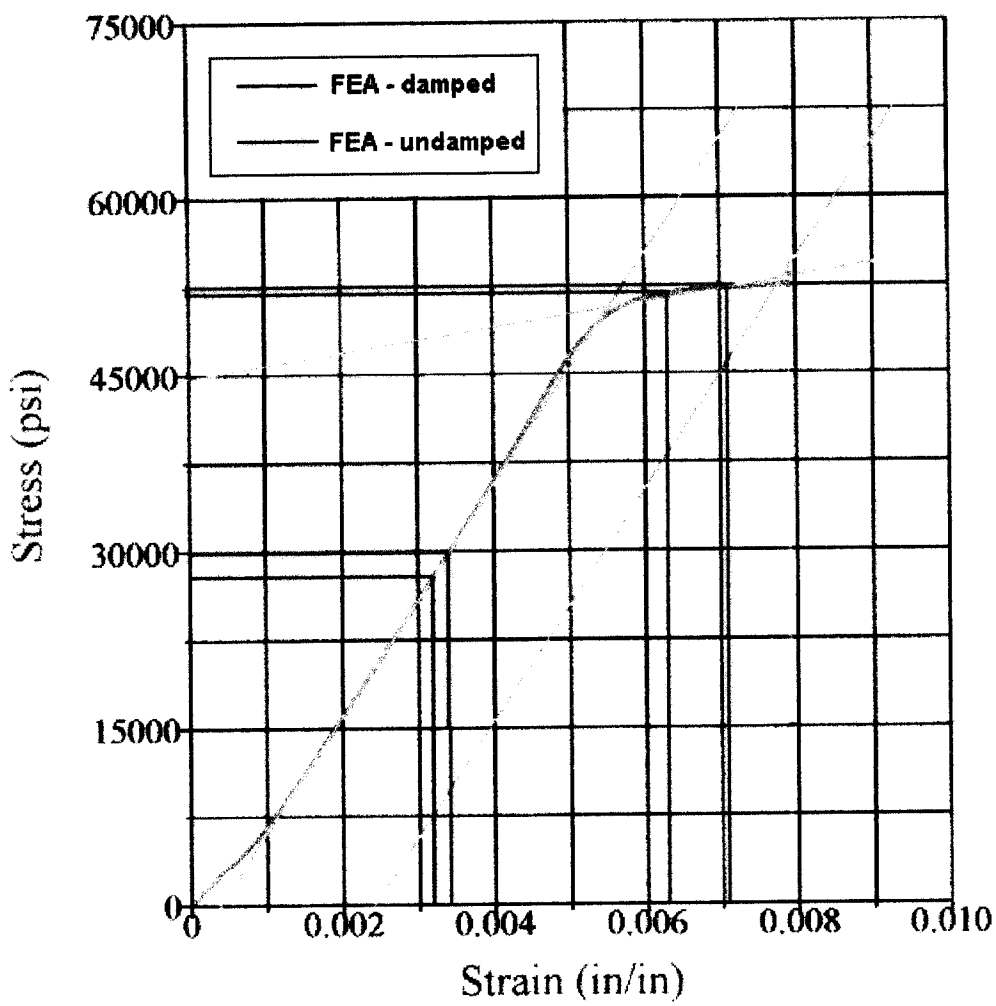


**Figure 6.1.1** - Stress vs. strain curve showing what FEA stress should be predicted based on the strain values FEA models predicted.

| | FEA - undamped | σ vs. ε curve | % Difference |
|---|---|---|---|
| Gage # 1 | 50,185 psi | ≈ 52,500 psi | 4.41 % |
| Gage # 2 | 30,998 psi | ≈ 30,000 psi | 3.21 % |

**Table 6.1.4** - Comparison of undamped FEA stress to values from σ vs. ε curve for the FEA predicted strain values.

| | FEA - damped $\alpha = 2.5, \beta = 0.5$ | σ vs. ε curve | % Difference |
|---|---|---|---|
| Gage # 1 | 50,918 psi | ≈ 51,000 psi | 0.16 % |
| Gage # 2 | 29,425 psi | ≈ 28,500 psi | 3.14 % |

**Table 6.1.5** - Comparison of damped FEA stress to values from σ vs. ε curve for the FEA predicted strain values.

| | FEA | Experimental | % Difference |
|---|---|---|---|
| Gage # 1 | 7044 με | 6255 με | 11.2 % |
| Gage # 2 | 3413 με | 2817 με | 17.5 % |

**Table 6.1.6** - Comparison of FEA with no damping to the average experimental results.

| | FEA | Experimental | % Difference |
|---|---|---|---|
| Gage # 1 | 6242 με | 6255 με | 0.21 % |
| Gage # 2 | 3190 με | 2817 με | 11.7 % |

**Table 6.1.7** - Comparison of FEA with damping to the average experimental results.

The percentage difference between the FEA models and the experimental results ranged from 0.16 - 17.5, with the greatest difference being in the FEA model with no damping as was expected. See Figure 6.1.2 for a comparison of the two FEA models and the experimental results. Notice how the experimental data intertwines with the damped and undamped FEA models in both the elastic and elasto-plastic regions.

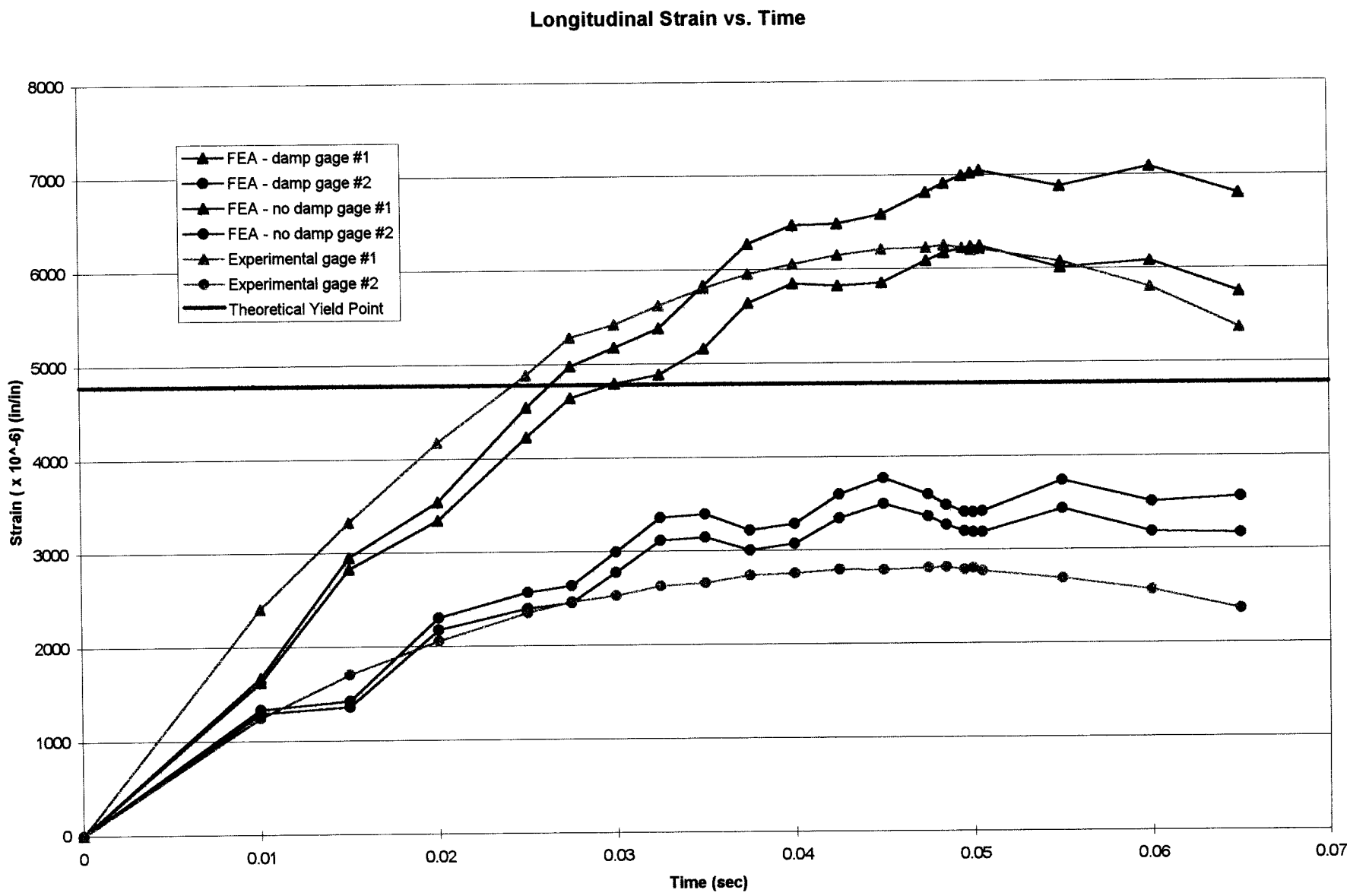


**Figure 6.1.2** - Graph of strain vs. time for the FEA models and experimental data

## 6.2 Conclusions

The amount of damping placed on the FEA model needs careful consideration. If the damping factor is set too high, the results for the model would be lower than expected, perhaps giving a false impression of the part's performance. However, if the damping is left out completely, the model should provide an approximate upper bounding limit, since in reality there always exists *some* damping of the system. Damping in reality is a function of the amount of yielding, frequency of strain waves, and other factors, but is not a constant. The software using a constant damping factor can then only be expected to approximate the actual damping involved in the impact. If the damping factor is carefully chosen, the approximation can closely represent reality as seen in Figure 6.1.2.

Overall, the nonlinear finite element analysis and event simulation proved to be an accurate tool for investigating post yield impact problems. The ability of the software to calculate and distribute the loading due to the motion of the system eliminates the need to find static equivalent loading and allows the problem to be solved dynamically, the way it actually occurs. The event simulation also provides an animated view of the system as the event unfolds, allowing the user to observe the system's full range of motion rather than a single static deflection.

# References

## Literary

Algor, Inc., Accupak / VE Reference Division - Revision 3.08., October 30, 1997.

Algor, Inc., Accupak / VE Reference Division - Appendix A: Input File Formats - Revision 3.08., October 30, 1997.

Algor, Inc., Accupak / VE Reference Division - Appendix B: Element Input File Formats - Revision 3.08., October 30, 1997.

Algor, Inc., Technical Staff, "The Theoretical Basis of Event Simulation.", Jan. 1998.

American Society for Testing and Materials, 1980 Annual Book of ASTM Standards: Part 10 Metals - Physical , Mechanical, and Corrosion Testing., Philadelphia. 1980.

Automotive Engineering International, May 1998, Vol. 106 No. 5, SAE International.

Avallone, Eugene A. and Buameister, Theodore III, Mark's Standard Handbook for Mechanical Engineers - Tenth Edition., McGraw-Hill, New York. 1996.

Burr, Arthur H and Cheatham, John B., Mechanical Analysis and Design - Second Edition., Prentice Hall, Englewood Cliffs, New Jersey. 1995.

Hibbler, R. C., Engineering Mechanics - Dynamics - Fifth Edition., MacMillan Publishing Company, Inc., New York. 1989.

Higdon, Archie; Stiles, William B.; et al., Mechanics of Materials - Fourth Edition., John Wiley & Sons, New York. 1985.

Juvinall, Robert C. and Marshek, Kurt M., Fundamentals of Machine Component Design - Second Edition., John Wiley & Sons, New York. 1991.

Thomson, William T., Theory of Vibration with Applications - Fourth Edition., Prentice Hall, Englewood Cliffs, New Jersey. 1993.

Vishay Measurements Group - Education Division, Bulletin 309D - Student Manual for Strain Gage Technology - A Brief Introduction and Guide to Selection, Installation, and Instrumentation., Measurements Group, Inc. 1992.

Van Vlack, Lawrence H., Elements of Materials Science and Engineering - Sixth Edition., Addison Wesley Publishing Company, New York. 1989.

Young, Warren C., Roark's Formulas for Stress & Strain - Sixth Edition., McGraw-Hill Inc., New York. 1989.

## World Wide Web / Internet

http://www.algor.com/

http://www.esi.fr/

http://www.measurementsgroup.com/

# Appendix A: Satec EMF 33 Tensile Tester Verification Sheets

# REPORT AND CERTIFICATE OF VERIFICATION

This certifies that the following described machine has been verified in accordance with ASTM E4-96 Force readings are within a tolerance of +/-1% & machine repeatability is less than or equal to 1%. TENSION

Location: SATEC Checkout

SATEC CDC Room

Manufacturer: SATEC Systems Inc
Model: 33EMF
Serial Number: CDC Room
Indicator Verified: APEX CRT
Machine Capacity: 33000.00 LBS.

Machine Range Verified: 99.00 to 990.00 Resolution: 0.10 LBS.

| Machine Reading | | Force | Device Reading | | Run 1 Machine Err. | | Run 2 Machine Err. | | Repeat- | CD |
|---|---|---|---|---|---|---|---|---|---|---|
| Run One | Run Two | % Diff. | Run One | Run Two | 1st. Err. | % | 2nd. Err. | % | ability | Code |
| 99.00 | 99.00 | 0.00% | 98.80 | 98.70 | 0.20 | 0.21% | 0.30 | 0.31% | 0.10% | 1 |
| 198.00 | 198.00 | 0.00% | 197.60 | 197.40 | 0.40 | 0.20% | 0.60 | 0.30% | 0.10% | 2 |
| 396.00 | 396.00 | 0.00% | 394.86 | 394.86 | 1.14 | 0.29% | 1.14 | 0.29% | 0.00% | 2 |
| 693.00 | 693.00 | 0.00% | 691.90 | 692.00 | 1.10 | 0.16% | 1.00 | 0.14% | 0.01% | 2 |
| 990.00 | 990.00 | 0.00% | 989.45 | 989.55 | 0.55 | 0.06% | 0.45 | 0.05% | 0.01% | 2 |
| 0.20 | 0.10 | Return to Zero | | | | | | | | |

Machine Range Verified: 990.00 to 9900.00 Resolution: 0.10 LBS.

| Machine Reading | | Force | Device Reading | | Run 1 Machine Err. | | Run 2 Machine Err. | | Repeat- | CD |
|---|---|---|---|---|---|---|---|---|---|---|
| Run One | Run Two | % Diff. | Run One | Run Two | 1st. Err. | % | 2nd. Err. | % | ability | Code |
| 990.00 | 990.00 | 0.00% | 989.45 | 989.55 | 0.55 | 0.06% | 0.45 | 0.05% | 0.01% | 2 |
| 1980.00 | 1980.00 | 0.00% | 1982.06 | 1982.26 | -2.06 | -0.10% | -2.26 | -0.11% | 0.01% | 2 |
| 3960.00 | 3960.00 | 0.00% | 3955.38 | 3950.38 | 4.62 | 0.12% | 9.62 | 0.24% | 0.13% | 4 |
| 6930.00 | 6930.00 | 0.00% | 6935.25 | 6930.25 | -5.25 | -0.08% | -0.25 | 0.00% | 0.07% | 4 |
| 9900.00 | 9900.00 | 0.00% | 9885.12 | 9880.12 | 14.88 | 0.15% | 19.88 | 0.20% | 0.05% | 4 |
| 1.50 | 3.30 | Return to Zero | | | | | | | | |

Machine Range Verified: 9900.0 to 33000.0 Resolution: 1.0 LBS.

| Machine Reading | | Force | Device Reading | | Run 1 Machine Err. | | Run 2 Machine Err. | | Repeat- | CD |
|---|---|---|---|---|---|---|---|---|---|---|
| Run One | Run Two | % Diff. | Run One | Run Two | 1st. Err. | % | 2nd. Err. | % | ability | Code |
| 9900.0 | 9900.0 | 0.00% | 9885.1 | 9880.1 | 14.9 | 0.15% | 19.9 | 0.20% | 0.05% | 4 |
| 19800.0 | 19800.0 | 0.00% | 19799.8 | 19804.8 | 0.2 | 0.00% | -4.8 | -0.02% | 0.03% | 4 |
| 33000.0 | 33000.0 | 0.00% | 32989.5 | 32984.5 | 10.5 | 0.03% | 15.5 | 0.05% | 0.02% | 4 |
| | | | | | | | | | | |
| | | | | | | | | | | |
| 1.5 | 3.3 | Return to Zero | | | | | | | | |

Method of verification and pertinent data on this certificate complies with the requirements of ASTM E4, ISO 10012-1, ANSI/NCSL Z540-1-1994, and ISO/IEC Guide 25-1990. Verification services were performed under a controlled Quality Assurance Program which incorporates the requirements of MIL-STD 45662A (SATEC Systems Service Department Q.A. Manual Rev. 1.0, 11/18/97. Calibration of the Verification devices used are traceable to the National Institute of Standards and Technology, (N.I.S.T.).

Date of Verification: 6/20/98
Due date: 6/20/99

Shawn Berkstresser
SATEC Service Engineer

Witness:

This Document shall not be reproduced without written approval of SATEC Systems, Inc.

Machine: SATEC Systems Inc
Model: 33EMF

Ser. No: CDC Room
Device Verified: APEX CRT

Machine Range Verified: to Resolution: LBS.

| Machine Reading | | Force | Device Reading | | Run 1 Machine Err. | | Run 2 Machine Err. | | Repeat- | CD |
|---|---|---|---|---|---|---|---|---|---|---|
| Run One | Run Two | % Diff. | Run One | Run Two | 1st. Err. | % | 2nd. Err. | % | ability | Code |
| | | | | | | | | | | |
| | | | | | | | | | | |
| | | | | | | | | | | |
| | | | | | | | | | | |
| | | | | | | | | | | |
| | | Return to Zero | | | | | | | | |

LOAD VALUES CORRECTED FOR A TEMPERATURE OF 72 DEGREES FAHRENHEIT.

VERFICATION METHOD USED:
X Follow-the-Force Method
____ Set-the-Force Method
____ Dead weights

SATEC MEASURING DEVICE INFORMATION

| C.D. Code | Serial Number | Manufacture | Verification High Value | Date Last Calibrated | Due Date | Range Class A | Traceable to NIST Lab No. |
|---|---|---|---|---|---|---|---|
| 1 | G587540B | REVERE | 500 | 04/28/98 | 04/28/99 | 6.92 | SJT.01/107061 |
| 2 | 73137 | BLH | 6,000 | 04/28/98 | 04/28/99 | 108.00 | SJT.01/107061 |
| 3 | G573292J | REVERE | 20,000 | 04/28/98 | 04/28/00 | 464.00 | SJT.01/107061 |
| 4 | G574210J | REVERE | 120,000 | 04/28/98 | 04/28/00 | 3,640.00 | SJT.01/107061 |
| 5 | | | | | | | |
| 6 | | | | | | | |
| 7 | Dead Wts. | RICE LAKES | 150 | 02/12/98 | 02/12/03 | 0.00 | 731/242697 |

Elastic verificatioin devices calibrated by National Standards Testing Laboratory in accordance with ASTM E74. Dead Weights certified by N/A in accordance with ASTM E4, paragraph (12.1).

Comments:

Cal Pt -21589
Range 1 95.00%
Range 2 95.00%
Range 3 95.30%
Range 4 95.71%

*To reschedule, please call 1-800-RAN-TEST (726-8378)*

*We sincerely appreciate your business and thank you for selecting SATEC Systems, Inc.*

# Appendix B: Algor Decoder Settings for FEA Models

# Appendix B: Algor Decoder Settings

The following are the specific decoder settings used for the two material groups used in the FEA model(s) in this study.

## Group 1 - The aluminum beam

**Element:**

type:

element 3-D:

(4) Von Mises - Isotropic hardening

info:

analysis:

(3) Updated Lagrangian Method

rS Integration:

(4) $4^{th}$ Order

t Integration:

(2) $4^{th}$ Order

group:

| | |
|---|---|
| Density: | $2.54e^{-4}$ |
| Young's: | $9.87e^{6}$ |
| Poisson's: | 0.3 |
| Rho y: | 47,167 |
| $E_t$: | $1.08e^{6}$ |

**Easy-Menu:**

Large Strain - Event Simulation: Motion

**Parameters:**

event simulation:

| | |
|---|---|
| SPS: | 2000 |
| EVTDUR: | 0.075 |

| | |
|---|---|
| timestep: | based on SPS above |
| * damping: | see footnote |

miscellaneous:

| | |
|---|---|
| RMEST: | 0.5 |
| IMASS: | 1 - lumped mass analysis |

**Curves:**

| | |
|---|---|
| load curves: | 2 points |

* Damping was changed for each model run. 1. No damping 2. Damping with $\alpha = 2.5$, $\beta = 0.5$

0,1 - @ time 0, load multiplier 1
0.075,1 - @ time 0.075, load multiplier 1
full load over entire event

gravities:

| | |
|---|---|
| LC: | 1 - load case # |
| DIR: | 3 - global Z direction |
| Lcurve: | 1- load curve # |
| Multiplier: | 386.4 - acceleration due to gravity |
| Apply: -1 - all | |
| Ax: | 0 |
| Ay: | 0 |
| Az: | -1 - unit vector of gravity |
| NG: | N/A |

centrifugal loads: none
impact walls: none

**Decode:**

higher-order elements: * - active

## Group 2 - The impacting mass

**Element:**

type:

element 3-D:

(1) Linear

info:

analysis:

(2) Total Lagrangian Method

rS Integration:

(2) 2nd Order

t Integration:

(2) 2nd Order

group:

| | |
|---|---|
| Density: | 0.0863 - with volume used = 6.25 lbs. |
| Young's: | $30e^6$ |
| Poisson's: | 0.3 |

**Easy-Menu:**

Large Strain - Event Simulation: Motion

**Parameters:**

initial:

| | |
|---|---|
| MODEX: | 1 |
| ICON: | 3 |

| | |
|---|---|
| $V_z$: | -39.31 |
| event simulation: | |
| SPS: | 2000 |
| EVTDUR: | 0.075 |
| timestep: | based on SPS above |
| ♦ damping: | see footnote |
| miscellaneous: | |
| RMEST: | 0.5 |
| IMASS: | 1 - lumped mass analysis |

**Curves:**

| | |
|---|---|
| load curves: | 2 points |
| | 0,1 - @ time 0, load multiplier 1 |
| | 0.075,1 - @ time 0.075, load multiplier 1 |
| | full load over entire event |
| gravities: | |
| LC: | 1 - load case # |
| DIR: | 3 - global Z direction |
| Lcurve: | 1- load curve # |
| Multiplier: | 386.4 - acceleration due to gravity |
| Apply: -1 - all | |
| Ax: | 0 |
| Ay: | 0 |
| Az: | -1 - unit vector of gravity |
| NG: | N/A |
| centrifugal loads: | none |
| impact walls: | none |

NOTE: In the Accupak / VE analyzer module, the strain output option was activated to obtain strain values to directly compare to the experimental electrical resistance strain gage readings.

♦ Damping was changed for each model run. 1. No damping 2. Damping with $\alpha = 2.5$, $\beta = 0.5$

# Appendix C: Laboratory Equipment Utilized

# Appendix C: Laboratory Equipment Utilized

Data acquisition unit:

SDA 2000 - Model #: SDA-2004
Serial #: 87071
YSU ID #: 51055

Personal computer:

EverEX 386 - 20 MHz
Model #: EX0-2804A-00
Serial #: EBY-11520043
YSU ID #: 53532

Monitor:

Seiko Instruments
Model #: CM-1440C
Type: CM-1440C-10
Serial #: OCM6549B

Strain Indicators:

Gage # 1: Vishay Measurements Group
Model #: 3800 Wide Range Strain Indicator
Serial #: 58990
YSU ID #: 46193

Gage # 2: Vishay Measurements Group
Model #: P-3500 Strain Indicator
Serial #: 60154
YSU ID #: 47177

Strain Gages:

Micro-measurements Division, Measurement Group, Inc.
All Gages Used: CEA-06-240UZ-120
Lot #: R-A56AD20
Code: 012016

Test Beams:

Micro-measurements Division, Measurement Group, Inc.

Aluminum Flexure Test Beams

Part #: 920-000-254

Surface Preparation Materials:

Micro-measurements Division, Measurement Group, Inc.

M-Line CSM-1 Degreaser

M-Prep Conditioner A

Part #: MCA-2

Control #: 502

M-Prep Neutralizer 5A

Part #: MN5A-2

Control #: 934

Adhesive:

Micro-measurements Division, Measurement Group, Inc.

M-Bond 200 Cyanoacrylate and Catalyst

Lead Wire:

Micro-measurements Division, Measurement Group, Inc.

M-Line Three Conductor Cable

Part #: 326-DFV

Solder:

Kester Solder

Part #: 24-6040-0018

Resin Core Alloy: 60/40

Dia.: 0.025

Core: 66

Soldering Station:

M-Line Mark V Soldering Station

YSU ID #: 34904

# CEA-Series Gages

## Description and Primary Application

Universal general-purpose strain gages. Constantan grid completely encapsulated in polyimide, with large, rugged copper-coated tabs. Primarily used for general-purpose static and dynamic stress analysis. 'C'-Feature gages are specially highlighted throughout the gage listings of Catalog 500.

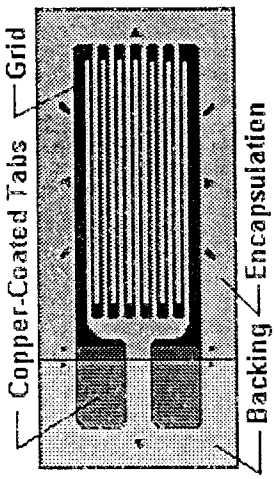


## Temperature Range

Normal: -100 deg to +350 deg F (-75 deg to +175 deg C)
Special or Short-Term: -320 deg to +400 deg F (-195 deg to +205 deg C)

## Strain Range

±3% for gage lengths under 1/8 in (3.2mm)
±5% for 1/8 in and over

## Fatigue Life

$10^5$ cycles at ±1500 microstrain
$10^6$ cycles at ±1500 microstrain with low modulus solder.

Micro-Measurements

# Strain Gage Accessories

## M-Bond 200 Adhesive

### Description

For routine experimental stress analysis applications under temperate environmental conditions, M-Bond 200 adhesive is ordinarily the best choice. This adhesive is very easy to handle, and cures almost instantly to produce an essentially creep-free, fatigue-resistant bond, with elongation capabilities of five percent, or more.

*M-Bond 200 Kit*

M-Bond 200 is a special cyanoacrylate which has been pretested and certified for use in bonding strain gages. It is an excellent general-purpose adhesive for laboratory and short-term field applications. The procedures are described in detail in Micro-Measurements Instruction Bulletin B-127, a copy of which accompanies each kit of adhesive.

The user should note that the performance of the adhesive can be degraded by the effects of time, humidity conditions, elevated temperature, and moisture absorption. Because of the latter effect, strain gage installations should always be covered with a suitable protective coating. When necessitated by more rigorous test requirements and/or environmental conditions, consideration should be given to one of the epoxy adhesives.

### Cure Requirements

One-minute thumb pressure, followed by a minimum two-minute delay before tape removal. Bond strength increases rapidly during first five minutes. Cure time must be extended under conditions of low temperatures [<70 deg F (<21 deg C)] or low humidity (<40% RH).

### Operating Temperature Range

Short Term: -300 deg to +200 deg F (-185 deg to +95 deg C)
Long Term: -25 deg to +150 deg F (-32 deg to +65 deg C)

### Elongation Capabilities

>6% at +75 deg F (+24 deg C), but 3% when used with CEA-Series or EA-Series/Option E gages.

## Shelf Life*

6 months at +75 deg F (+24 deg C) (After opening, and properly sealing after each application.)
9 months at +75 deg F (+24 deg C); 12 mo at +40 deg F (+5 deg C) (Unopened adhesive only.)

## Instruction Manual

B-127

---

## Ordering Information

- **M-Bond 200 Kit** (as shown above) with 1 bottle [1 oz (28 gm)] Adhesive, 1 brush-cap bottle (30ml) Catalyst, polyethylene dispenser cap.
- **M-Bond 200 Bulk** includes 16 bottles [1 oz (28 gm)] Adhesive, 12 brush-cap bottle (30ml) Catalyst.

---

* Shelf life refers to the duration of time, beginning with the date of shipment, over which the item, when properly stored, should be expected to meet published specifications.

# Teaching & Learning Aids

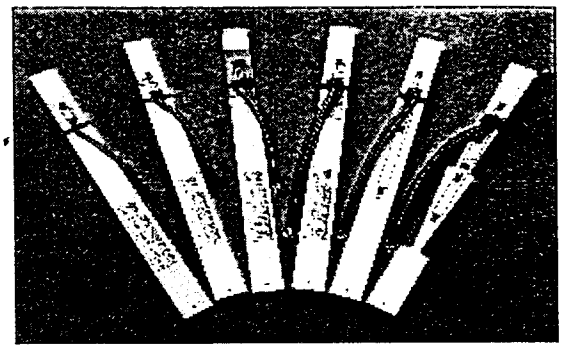

## Cantilever Beams

Designed for use with the Flexor, Cantilever Beams are coordinated with Experiments in Mechanics, but can be used separately for other demonstrations or experiments. All beams are manufactured from 2024-T6 high-strength aluminum alloy and are 1 in (25.4 mm) wide by 12.5 in (3175 mm) long. Beams designed for Experiments E-101 and E-103 are 0.125 in (3.18 mm) thick. All others are 0.250 in (6.35 mm) thick.

### Ungaged Beams

Ungaged Beams permit specialized instruction and are particularly valuable when instructional time is sufficient to allow students to mount their own strain gages. Experiments in Mechanics available separately.

### Special Configuration Beams

Special Configuration Beams are designed for advanced work in measuring stress concentrations. They are ungaged to afford students the opportunity to position and mount their own strain gages. Experiments in Mechanics available separately.

### Pregaged Beams

Pregaged Beams are instrumented with Micro-Measurements temperature-compensated foil strain gages. The strain gage installations are fully wired and are covered with a clear protective coating. In addition, all installations are factory tested for resistance, stability, and freedom from creep. Beams ship with a copy of the corresponding Experiments in Mechanics.